THE JOURNAL OF PHYSICAL CHEMISTRY A

Article

pubs.acs.org/JPCA

Rotation Dynamics Do Not Determine the Unexpected Isotropy of Methyl Radical EPR Spectra

Nikolas P. Benetis,*[,†] Yurij Dmitriev,[‡] Francesca Mocci,[§] and Aatto Laaksonen[∥]

[†]Department of Environmental Engineering and Antipollution Control, Technological Educational Institute of Western Macedonia (TEI), Kila 50 100 Kozani, Greece

[‡]Ioffe Institute, 26 Politekhnicheskaya ul., 194021 St. Petersburg, Russia

[§]Dipartimento di Scienze Chimiche e Geologiche, Università di Cagliari, Via San Giorgio 12/2, 09124 Cagliari, Italy

[∥]Division of Physical Chemistry, Department of Materials and Environmental Chemistry, Arrhenius Laboratory, Stockholm University, 106 91 Stockholm, Sweden

Supporting Information

ABSTRACT: A simple first-principles electronic structure computation, further qc (quantum chemistry) computation, of the methyl radical gives three equal hf (hyperfine) couplings for the three protons with the unpaired electron. The corresponding dipolar tensors were notably rhombic and had different orientations and regular magnitude components, as they should, but what the overall **A**-tensor was seen by the electron spin is a different story! The final **g** = (2.002993, 2.002993, 2.002231) tensor and the hf coupling results obtained in vacuum, at the B3LYP/EPRIII level of theory clearly indicate that in particular the above **A** = (−65.19, −65.19, 62.54) MHz tensor was axial to a first approximation without considering any rotational dynamics for the CH_3. This approximation was not applicable, however, for the trifluoromethyl CF_3 radical, a heavier and nonplanar rotor with very anisotropic hf coupling, used here for comparison. Finally, a derivation is presented explaining why there is actually no need for the CH_3 radicals to consider additional rotational dynamics in order for the electron to obtain an axially symmetric hf (hyperfine) tensor by considering the simultaneous dipolar couplings of the three protons. An additional consequence is an almost isotropic **A**-tensor for the electron spin of the CH_3 radical. To the best of our knowledge, this point has not been discussed in the literature before. The unexpected isotropy of the EPR parameters of CH_3 was solely attributed to the rotational dynamics and was not clearly separated from the overall symmetry of the species. The present theoretical results allowed a first explanation of the "forbidden" satellite lines in the CH_3 EPR spectrum. The satellites are a fingerprint of the radical rotation, helping thus in distinguishing the CH_3 reorientation from quantum rotation at very low temperatures.

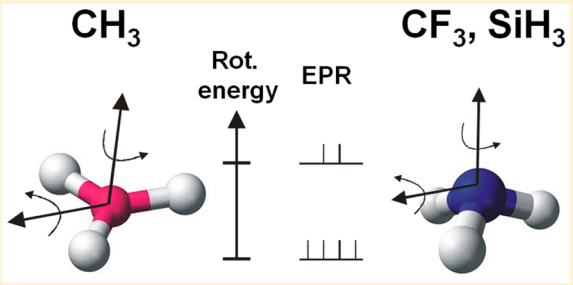

INTRODUCTION

In this work we attempt to simulate the EPR lineshapes of the CH_3 radical with the magnetic parameters obtained from DFT computations using the Gaussian software and compare with the experimental EPR spectra obtained in several scientific efforts concerning that simple but extremely interesting system. In spite that the present quantum chemistry (qc) computation is of the simplest kind, i.e., in vacuum, it agrees rather well with the experimental spectra of CH_3 in solid matrices, preserving the relative magnitudes and the orientations of the relevant anisotropic magnetic parameters. In particular, the **g**-tensor electron Zeeman and the **A**-tensors of the protons' hf interaction with the electron spin were faithfully reproduced.

It is thus very interesting to notice first that the qc-computation agrees with the theoretical predictions about the hf coupling for methyl radical; see Figure 1. They confirm the negative sign and the relative magnitude of the Fermi contact term with respect to the dipolar tensor components and the orientation with respect to the a >C$^{\bullet}$−H fragment. Such is also the case for the benzene ring protons and in general alpha protons coupled to unpaired electrons on p- or π-orbital of the neighboring carbons.

As seen in Figure 1, for the traceless part of the dipolar interaction, one expects a max positive dipolar coupling of ca. 10 G along the direction of the proton, while along the direction of the p_z orbital the interaction is negligible. On the other hand perpendicular to these directions, i.e., the p_z orbital and the C−H bond, a negative dipolar coupling of equal magnitude to the C−H bond direction is approximately expected.

Summing up further, the well-known spin polarization effect seen graphically in Figure 2. In the α-state of the unpaired electron, the coupled proton spin obtains a slight excess of β electron spin polarization leading to negative sign to the Fermi

Received: June 13, 2015
Revised: August 7, 2015
Published: August 11, 2015

DOI: 10.1021/acs.jpca.5b05648
J. Phys. Chem. A 2015, 119, 9385−9404

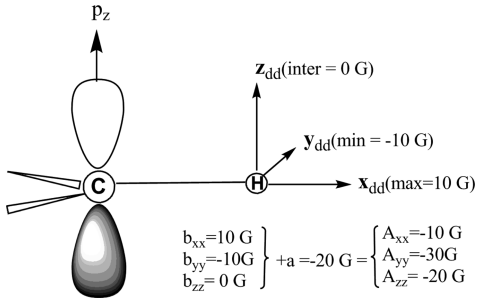

Figure 1. Approximate theoretical predictions for the hf coupling of a >C•p_z-H fragment with the p_z orbital in the carbon atom bound to an alpha proton.[1−3] The isotropic Fermi contact interaction is negative due to spin polarization, while the *x*- and *y*-components of the dipolar interaction are equal and opposite in sign. The pure dipolar interaction along the p_z axis is insignificant in value.

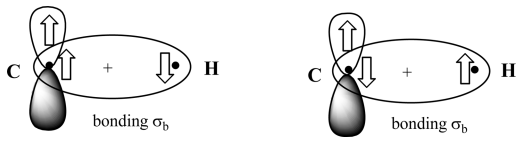

Figure 2. Spin polarization mechanism. The possible orientations of the spins in the C−H bond in relation to the spin orientation of the p-orbital of the C atom. The left configuration is slightly more stable.

contact term, see in the book from Carrington and McLauchlan.[3]

The Gaussian output contains 3 hfc (hyperfine coupling) anisotropic components, with different direction cosines for each of them. In agreement with the qc-computations the hf splitting is rhombic for each proton, and the three protons are arranged around the p_z-orbital symmetrically. The EPR properties of the electron spin $S = 1/2$ doublet interacting with the three protons must reflect this situation. Utilization of the coupled nuclear spin representation leads to a simpler lineshape computation, vide infra, at least the totally symmetric nuclear quartet involved in the hf interaction must be overall axially symmetric and diagonal in the molecular frame to conform to the $\mathbf{D}_3$ symmetry of the molecule.

The two additional, not fully symmetric, *E*-doublets in the largest abelian $\mathbf{C}_3$ group of the radical figure do not necessarily need to be diagonal in the molecular frame, however. For the planar CH_3 radical within $\mathbf{C}_3$, the doublets did not deviated significantly from being diagonal in the molecular framework. On the contrary the assumption of parallel axes of all the nuclear spin multiplets for CF_3 will not account for the central part of the experimental spectra, unless, as shown further in the theoretical part, the two additional doublets mentioned above are reoriented carefully. Of course, the powder EPR spectrum of CH_3 and in particular of CF_3 can always be reproduced by numerical simulations assuming nonparallel although symmetry-related directions of the principal axes for the three anisotropic ^{19}F hf interactions. This is different to the problem that was encountered in the quantum rotation of methyl in Ar where the nuclear spin couples to rotation, by Yamada and Benetis et al.[4] A similar problem was more recently studied by Lon Knight's group,[5] while analyzing Ne matrix isolated H_2^+ and D_2^+ EPR results. In case of H_2^+, for example, the EPR spectrum clearly demonstrates quantum effect being a superposition of a triplet (nuclear spin triplet $I = 1$) and an unsplit electronic transition (nuclear spin $I = 0$). Thus, despite the quenched, three-dimensional free rotation, the nuclear spin function of the molecular ion H_2^+ couples to the libration states in order to obtain the overall antisymmetric "electronic-libration-nuclear" wave function required by the Pauli principle.

A rotating beta-proton methyl fragment on the other hand should behave as axially symmetric and almost as magnetically isotropic; see Benetis and Dmitriev for the basic definitions of methyl rotors.[6] Freed was the first to study in detail the tunneling of such a rotating methyl fragment of a larger molecular unit,[7] at least for low temperature.

In our case of static molecules the powder EPR simulations do not need to account for the "nuclear spin−rotation" coupling. In cases, such as CH_3 (planar molecule), SiH_3, and the CF_3 (pyramidal molecules), the experimental EPR results will be obtained by attempting a reorganization of the nuclear spins within the minimal $\mathbf{C}_3$ symmetry. A particular aim is the reproductions of the observation of Maruani et al.[8,9] of CF_3 in Kr and Xe.

It will accordingly be suggested that there is no need for dynamical rotational averaging for previous interpretations of the unexpected isotropy of the hf tensor of the CH_3 radical. That is also probably why very few papers, except Kubota,[10] never observed any rhombic anisotropy in CH_3.

It is not known in the literature any experimental rigid limit rhombic powder spectrum of methyl. The paper by Kubota et al.[10] is concerning a single crystal sample.

It is not then so strange that nobody ever observed what Kubota's et al.[10] data indicate, i.e., a powder spectrum resembling a rhombic hf- tensor accounting for the *A*-state quartet. We exclude naturally the EPR satellites of "non-rotating" methyls recently observed by us and other groups as remnants of the powder spectrum resembling to a rhombic *hf*-tensor, vide infra.

The system they study is probably not an intact free methyl. Actually they rather observe a >C•-H fragment of a larger species that contain the unpaired electron and minimal motional degrees of freedom. In any case it seems necessary to compare to the Kubota's original interpretation since they seem to record the EPR spectrum of a single motionless >C•-H fragment and not the full CH_3.

Most of the relevant articles show that the overall powder EPR spectrum is axially symmetric according to the positions of the three protons dictated by the $\mathbf{D}_3/\mathbf{C}_{3v}$ symmetry. The present computation of the accumulated hf coupling of the three protons on the electron shows that beyond any doubt. This result brings about a simple explanation for the unusual isotropy of the EPR lineshape of methyl radical, not involving the coupling to the radical rotation, thus changing the accepted model which lasts from the article by Lee and Rogers[11] in the middle of the 1970s.

We consider this question important, in order to explain the long-standing irregularity of methyl radical: a researcher always recording an almost isotropic EPR lineshape. This will also raise the question why some few groups, e.g., Kubota's and to a lesser extent Brustolon's group[12] reports, involve orthorhombic hf coupling.

A straightforward powder EPR simulation procedure of methyl CH_3 radicals is to consider the interaction of the three different protons separately one after the other applying consecutive splitting of the electrons spin by the three protons by convolution. In particular, the hfc of each H would differ at most a single crystal orientations, giving 2 × 2 × 2 ESR lines, quite different from a single H. Concerning also the situation of

DOI: 10.1021/acs.jpca.5b05648
J. Phys. Chem. A 2015, 119, 9385−9404

cryogenic temperatures, one should perform similar calculations and EPR simulations for CF_3 as a test of the method. A simulated CF_3 spectrum is an example in *EasySpin* documentation. The program is free software written by S. Stoll in Matlab.[13] A comparison to the heavy radical CF_3, which cannot tunnel, would show the difference only at very low temperatures. Notice, e.g., the computed over 25-fold greater rotational frequencies of the CH_3 in the next section.

Two simpler alternative ways of the spectral simulation were employed in the present work by consideration of an overall hf coupling of the three protons with the electron from the beginning.

(1) A superposition of the appropriately averaged quartet and a doublet with the same parameters.
(2) A similar superposition of a quartet and two doublets, further mentioned as the 1Q/2D method, with hf parameters dictated by the radical symmetry.

The planar CH_3 was easily simulated by considering the superposition of the spatially averaged quartet and the two doublets separately, while the more anisotropic and pyramidal CF_3 requires a more careful simultaneous superposition.

THEORETICAL SECTION

Quantum Chemistry Computation of the Magnetic Parameters. *The Methyl CH_3 Radical.* The B3LYP/EPR-III method was used to run the methyl CH_3 and the trifluoromethyl CF_3 radical optimizations in vacuum with *Gaussian 09* and to compute the **g**- and **A**-tensors.[14] The basis set—EPR-III, optimized for the computation of hyperfine coupling constants by DFT methods, particularly B3LYP—is a triple-ζ basis set including diffuse functions, double d-polarizations, and a single set of f-polarization functions; see Table 1. Also in this case the s-part is improved to better describe the nuclear region.

Table 1. Computed Atomic Cartesian Coordinates and Rotational Constants for the CH_3 Radical

atom	X (Å)	Y (Å)	Z (Å)
^{13}C	0.000000	0.000000	0.000417
H(1)	0.000000	1.078501	−0.000833
H(2)	−0.934010	−0.539251	−0.000833
H(3)	0.934010	−0.539251	−0.000833
rotational constants (GHz)	287.5221312	287.4868166	143.7522364

The optimization converged fast and showed a planar and totally symmetric CH_3 radical within the $\mathbf{C}_{3v}/\mathbf{D}_3$ group and the C−H distance 1.0785 Å. Actually, the $\mathbf{D}_3$ group is the appropriate one for the planar geometry of the CH_3 species.

The **g**-tensor computation includes: relativistic mass correction, diamagnetic correction, orbital Zeeman, and spin−orbit coupling contribution, all summed to the tensor **g** = (2.0029929, 2.0029930, and 2.0022307).

Two earlier density functional computations reported axially symmetric **g**-tensor of the CH_3 radical in vacuum. The results by Schreckenbach and Ziegler,[15] $g_{\|}$ = 2.002228 and $g_{\perp}$ = 2.003069, are very close to those computed in this work: $g_{\|}$ = 2.002231 and $g_{\perp}$ = 2.002993. On the other hand, Vahtras et al.[16] applied the atomic mean-field approximation (AMFI) to the spin−orbit interaction Hamiltonian in evaluating the paramagnetic contribution to the electronic **g**-tensor, providing a different sets of parameters, i.e., $g_{\|}$ = 2.00232 and $g_{\perp}$ = 2.00279.

The transformation axes for the first proton were left-handed, including an inversion, so the direction of one or three of the axes had to be changed. In this particular case the *x*-axis was changed; see further. The other two tensors were rotated properly.

The computed molecular model in Figure 3 shows that there is full agreement with the expected tensor orientation shown in

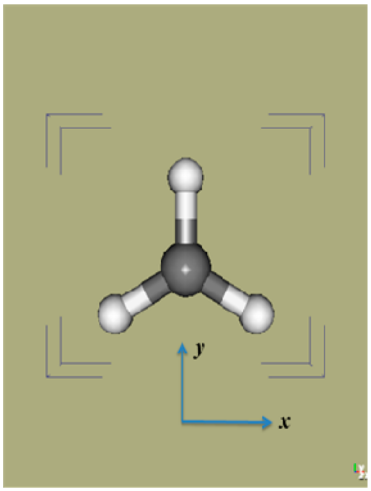

Figure 3. CH_3 radical in the *xy*-plane determined by the Gaussian. The **g**- tensor in that reference system is diagonal and has the components $g_{xx} = g_{yy}$ = 2.0029930, g_{zz} = 2.002231. The **g**-tensor is thus axial with $\Delta g = g_{\|} - g_{\perp} = -7.62 \times 10^{-4}$, and the *g*-factor value is 2.002739.

Figure 1. Take for example the proton nr. one that is bound along the molecular *y*-axis. The *y*-axis is the direction along the C−H bond that must have a positive DD-interaction value ca. + 10 G; the computed value 13.76 G. This is actually true as seen by the direction cosine matrix that exchanges the molecular *y*- and *z*-axes. Simultaneously the *z*-axis which has DD-interaction value close to zero was computed to 0.476 G as it should. Finally, the remaining *x*-axis perpendicular to *y* and *z* has the appropriate negative value −10 G, computed to −14.23 G. The Bruker *WinEPR* software and also the *EasySpin* software were applied in the simulation procedure. The isotropic, Fermi contact, coupling of each of the three protons was a_{iso} = −23.01966 G (1 Gauss = 2.802 MHz).

As in the case of ENDOR, at each proton the effect of the hf coupling is simpler than the effect of the sampled couplings of the rest of the protons and the magnetically active neighbors in general. The anisotropic dipole−dipole couplings from the electron to all three methyl protons are unique and have the identical values as above. We suggest that the simultaneous hf effect of these three protons on the electron can be computed by assuming that the electron distribution is split equally to them and therefore each contributes to the hf interaction by 1/3.

Accordingly, we consider identical anisotropic parts of the hf interaction but three different orientations of the corresponding **A**- tensors; see Table 2.

As an example, for the first proton, we sum the above traceless part of the anisotropic spin dipole couplings to the Fermi contact part in order to obtain the total hf-interaction tensor.

DOI: 10.1021/acs.jpca.5b05648
J. Phys. Chem. A 2015, 119, 9385−9404

Table 2. Computed Isotropic (Fermi) and Anisotropic Spin Dipole Couplings in the Principal Axis System of the CH_3 Radical

	atom	MHz	Gauss	axes (directions cosines)[a]		
isotropic hfi	^{13}C	80.26397	28.64018			
	H(1,2,3)	−64.51248	−23.01966			
atom						
H(1)	A11	−39.884	−14.231	1.0000	0.0000	0.0000
	A22	1.334	0.476	0.0000	0.0014	1.0000
	A33	38.549	13.755	0.0000	1.0000	−0.0014
H(2)	A11	−39.884	−14.231	−0.5000	0.8660	0.0000
	A22	1.334	0.476	−0.0012	−0.0007	1.0000
	A33	38.549	13.755	0.8660	0.5000	0.0014
H(3)	A11	−39.884	−14.231	0.5000	0.8660	0.0000
	A22	1.334	0.476	0.0012	−0.0007	1.0000
	A33	38.549	13.755	0.8660	−0.5000	−0.0014

[a]The transposes of the matrices are identified with the direction cosines and are further transformed to Euler angles.

For H(1) the anisotropic and traceless part of the hf tensor is $\mathbf{A}^{(0)}$ = (−14.231, 0.476, 13.755) Gauss.

The total hf tensor, including the Fermi contact term A_{iso} = −23.01966, is thus for the H(1) proton in the principal frame $\mathbf{A}_1$ = (−37.251, −22.544, −9.265) Gauss = (−104.4, −63.17, −25.96) MHz. This tensor is very close to the expected one for an alpha proton regarding the regular values of Figure 1, if the components are rearranged as $\mathbf{A}_{1,regular} \approx (A_{1,yy}, A_{1,zz}, A_{1,xx})$ Gauss. This particular orientation of this tensor in the molecular frame is determined by the following direction cosines.

$$\mathbf{R}'_1 = \begin{pmatrix} 1.000 & 0.000 & 0.000 \\ 0.000 & 0.0014 & 1.000 \\ 0.000 & 1.000 & -0.0014 \end{pmatrix}$$

with respect to the standard molecular frame of the Gaussian computation shown in Figure 3.

The transpose matrices to the above ones obtained by the qc (quantum chemistry) computations are further identified to the direction cosines, as the qc relate the rows of these matrices to the principal values of the hf interaction. In this case of a symmetric transformation matrix, no doubt is raised with respect to the correct definition of the direction cosines as transpose or not.

Obviously this $\mathbf{R}'_1$ transformation indicates that the *y*- and *z*-components must be exchanged. This is equivalent to the Euler angles $\mathbf{R}'_1$ = (90.00, 89.92, −90.00) degrees, which means that the principal frame of the hf tensor for the H(1) proton is rotated by 90° (the exact value is 89.92°, obviously due to numerical lack of accuracy or small planarity deviation) about the negative *x*-axis. This is actually happening if one checks the matrix $\mathbf{A}_1$ in the following. However, an extra difficulty is noticed in this transformation being an improper rotation involving an extra inversion. Let then invert the direction of the *x*-axis in the above rotation matrix $\mathbf{R}_1$ and obtain

$$\mathbf{R}_1 = \begin{pmatrix} -1.000 & 0.000 & 0.000 \\ 0.000 & 0.0014 & 1.000 \\ 0.000 & 1.000 & -0.0014 \end{pmatrix}$$

The corresponding, new Euler angles obtained, $\mathbf{R}_{1R}$ = (90.00, 90.08, −90.00) are almost identical as above, giving also the same transformed tensor in the molecular frame seen in the following.

This and similar computations in the following were performed by a small in-house-made program which transforms the direction cosines in the equivalent but shorter representation of Euler angles and give a representation of each second rank tensor in the molecular frame, here the standard frame determined by *Gaussian 09*.[14]

The protons H(2) and H(3) have the same as the above nominal traceless part $\mathbf{A}^{(0)}$, and total hf tensors components but different orientations described simplest by the following Eulers: $\mathbf{R}_2$= (90.00, 89.92, 150) degrees and $\mathbf{R}_3$ = (90.00, 90.00, −150) degrees, respectively.

These rotations refer to the frame shown in the above Figure 3 determined by the standard orientation of the radical as it was computed by the Gaussian.

The Cartesian $\mathbf{A}_1$ to $\mathbf{A}_3$ Tensors. In the same, standard frame of the quantum chemistry computation seen in Figure 3, the three dipolar tensors of the protons can be represented as in the following 3 × 3 matrices.

$$\mathbf{A}_1 = \begin{pmatrix} -37.251 & 0.0000 & 0.0000 \\ 0.0000 & -9.265044 & -1.859 \times 10^{-2} \\ 0.0000 & -1.859 \times 10^{-2} & -22.544 \end{pmatrix} \text{Gauss}$$

Eulers $\mathbf{R}'_1$ = (90.00, 89.92, −90.00) for the left-handed; $\mathbf{R}_{1R}$ = (90.00, 90.08, −90.00).

$$\mathbf{A}_2 = \begin{pmatrix} -16.2611 & 12.11795 & 1.5495 \times 10^{-2} \\ 12.11795 & -30.253 & 9.3747 \times 10^{-3} \\ 1.5495 \times 10^{-2} & 9.3747 \times 10^{-3} & -22.198 \end{pmatrix}$$

Gauss

$\mathbf{R}_2$ = (90.00, 89.92, 150.0) degrees and

$$\mathbf{A}_3 = \begin{pmatrix} -16.2611 & -12.11795 & -1.5495 \times 10^{-2} \\ -12.11795 & -30.253 & 9.3747 \times 10^{-3} \\ -1.5495 \times 10^{-2} & 9.3747 \times 10^{-3} & -22.198 \end{pmatrix}$$

Gauss

$\mathbf{R}_3$ = (90.00, 90.00, −150.0) degrees, respectively.

The above orientation data indicate a planar radical and locates the three tensors in the molecular plane, with different *x*, *y*-orientations for the three **A** tensors.

Adding the three **A** tensors in order to obtain the overall contribution of all three protons:

DOI: 10.1021/acs.jpca.5b05648
J. Phys. Chem. A 2015, 119, 9385−9404

$$\mathbf{A}_{tot} = \begin{pmatrix} -69.773 & 0.000 & 0.000 \\ 0.000 & -69.77 & 1.59 \times 10^{-4} \\ 0.000 & 1.59 \times 10^{-4} & -66.939 \end{pmatrix} \text{Gauss}$$

One has to average the above values.

$$\mathbf{A}_{H} = \begin{pmatrix} -23.258 & 0.000 & 0.000 \\ 0.000 & -23.257 & 5.29 \times 10^{-5} \\ 0.000 & 5.29 \times 10^{-5} & -22.313 \end{pmatrix} \text{Gauss}$$

Based on this result, we obtain for the isotropic coupling: A_{iso} = −22.943 G. This value is close to the experimental −23.37 G.

Of course the hf interaction of the C-13 with the electron would be immediately axial and coinciding in direction with the **g**-tensor and the above computed $\mathbf{A}_H$, vide infra.

A simulation of the EPR powder of the rigid methyl radical is shown in Figure 4, which is performed using the *EasySpin* software. Axially symmetrical **A**- and **g**-tensors were assumed based on the above qc-computations of the $\mathbf{A}_H$ and **g**-tensors. The figure demonstrates a technique of the simulation of the methyl radical EPR utilized in the present study. Figure 4a presents the quartet attributable to the radical CH_3 **A**-state, while a doublet in Figure 4b stands for the *E*-state radicals. Both multiplets are simulated with equal EPR parameters. Figure 4c shows a superposition of the quartet and doublet with equal weights expected in the high-temperature limit when all rotation levels of the radical are equally populated.

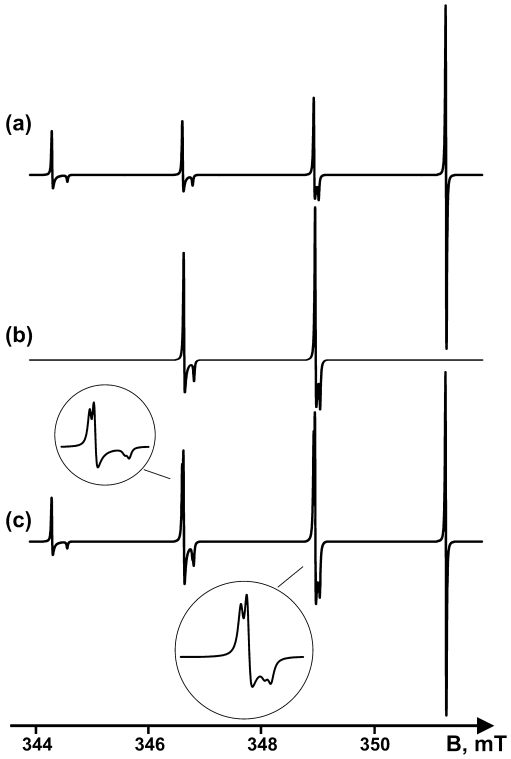

Figure 4. Simulation of the EPR powder of the rigid methyl radical using the *EasySpin* software.[13] Axially symmetrical **A**- and **g**-tensors were assumed, $g_{\|}$ = 2.002231, $g_{\perp}$= 2.002993, and $A_{\|}$ = −62.54 MHz, $A_{\perp}$ = −65.19 MHz. The individual lines were convoluted with isotropic Lorentzians 0.015 mT wide. The high-temperature condition was assumed fulfilled, i.e., the populations of the *A*- and *E*-symmetry states were equal. Here, (a) *A*-state quartet, (b) *E*-state doublet with identical parameters as above, (c) superposition of the *A*- and *E*-state spectra. Microwave resonance frequency, f_{res} = 9750.00 MHz. Insets show details of the M_F = 1/2 and M_F = −1/2 hf component lineshape.

However, the full theory given in the following identifies the above summation of the hf tensors to the main part, i.e., to the quartet **Q** of the symmetrized spin Hamiltonian in the $\mathbf{C}_3$ group, while in addition the hf parameters of the doublets are recalculated to conform to the *E*-symmetry.

In spite that the qc-computation of the hf coupling was performed using second-order perturbation,[17] the above summation of the hf interactions of each proton to a total effect on the electron does not correspond exactly to the total anisotropic hf Hamiltonian,

$$H^{(hf)} = \mathbf{I}_1 \cdot \mathbf{A}_1 \cdot \mathbf{S} + \mathbf{I}_2 \cdot \mathbf{A}_2 \cdot \mathbf{S} + \mathbf{I}_3 \cdot \mathbf{A}_3 \cdot \mathbf{S} \quad (1)$$

because the nuclear part

$$\mathbf{V}(\text{hf}) = \sum_{i=1}^{3} \mathbf{A}_i \cdot \mathbf{I}_i \quad (2)$$

considered as a vector, consists of three different vectors pointing at different directions.

As it will be shown further in the theoretical part, two additional doublets of different hf strength and orientation characteristics have to be simultaneously superimposed within the appropriate symmetry group of the radical.

Furthermore, it will be shown that the orientation of the two *E*-doublets in the molecular frame conforms to the planarity of the radical.

Except for the two radicals treated here, i.e., the methyl CH_3 and the trifluoromethyl CF_3, some other hydrides of group IV in the periodic table,[18] such as the SiH_3, belonging also to the same category, behaving almost as CH_3. In particular the assumed nonplanar SiH_3 radical demonstrates axially symmetric EPR even at very low temperatures. The controversy about the planarity vs EPR properties of the species may be resolved by the proposed method in the present work.

The Trifluoromethyl CF_3 Radical. From the computed structure in Table 3, the spatial parameters for the CF_3 radical

Table 3. Computed Atomic Cartesian Coordinates and Rotational Constants in the CF_3 Radical

atom	*X* (Å)	*Y* (Å)	*Z* (Å)
^{13}C	0.000000	0.000000	0.324341
$^{19}F(1)$	0.000000	1.259899	−0.072076
$^{19}F(2)$	−1.091104	−0.629949	−0.072076
$^{19}F(3)$	1.091104	−0.629949	−0.072076
rotational constants (GHz)	10.8002416	10.8002416	5.5860844

are obtained: C−F distance = 1.3208 Å, F−C−F angle = 111.4°. Obviously the radical is pyramidal (Figure 5 higher), in contrast to the planar methyl radical.

The computed **g**-tensor for the CF_3 radical in vacuum by including the relativistic mass correction, the diamagnetic correction, and the orbital Zeeman and spin−orbit coupling contributions result to **g** = (2.0042442, 2.0042458, 2.0016636), giving a *g*-factor = 2.0033845 and $\Delta g = g_{\|} - g_{\perp} = -2.2814 \times 10^{-3}$.

The transformation axes for the **A**-tensor of the first fluorine nucleus, Table 4, were not corresponding to proper rotation—they included an inversion—so the sign of one or three axes

DOI: 10.1021/acs.jpca.5b05648
J. Phys. Chem. A 2015, 119, 9385−9404

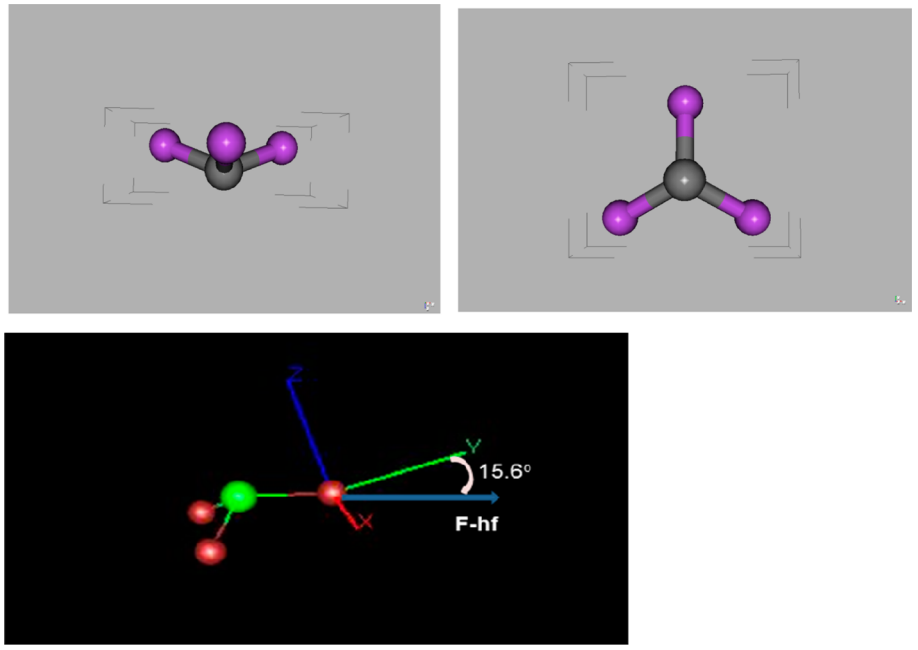

Figure 5. Higher: Optimized structure of CF_3 radical. Left: *y*-axis in the front. Right: *z*-axis in the front. Lower: The Gaussian computation standard coordinate frame compared to the anisotropic hf interaction tensor of a fluorine atom. The relative direction of the *y*-component of the molecular frame (green arrow) is seen vs the F-hf interaction tensor component (blue arrow).

Table 4. Computed Isotropic (Fermi) and Anisotropic Spin Dipole Couplings in the Principal Axis System of the CF_3 Radical[a]

	atom	MHz	Gauss	axes (directions cosines)		
isotropic hfi	^{13}C	740.37920	264.18570			
	$^{19}F(1,2,3)$	387.65397	138.32457			
atom						
^{13}C	A11	−68.292	−24.368	0.9982	−0.0601	0.0000
	A22	−68.292	−24.368	0.0601	0.9982	0.0000
	A33	136.584	48.737	0.0000	0.0000	1.0000
$^{19}F(1)$	A11	−204.455	−72.955	0.0000	0.9631	0.2690
	A22	−194.056	−69.244	1.0000	0.0000	0.0000
	A33	398.511	142.199	0.0000	−0.2690	0.9631
$^{19}F(2)$	A11	−204.455	−72.955	0.8341	0.4816	−0.2690
	A22	−194.056	−69.244	−0.5000	0.8660	0.0000
	A33	398.511	142.199	0.2330	0.1345	0.9631
$^{19}F(3)$	A11	−204.455	−72.955	0.8341	−0.4816	0.2690
	A22	−194.056	−69.244	0.5000	0.8660	0.0000
	A33	398.511	142.199	−0.2330	0.1345	0.9631

[a]The transposes of the matrices are identified with the direction cosines and are further transformed to Euler angles.

have to be changed. Changing the sign of the *x*-axis of the first fluorine,

$$\mathbf{R}_{1R} = \begin{pmatrix} 0.000 & 0.9631 & 0.2690 \\ -1.000 & 0.000 & 0.000 \\ 0.000 & -0.2690 & 0.9631 \end{pmatrix}$$

The transformation $\mathbf{R}_{1R}$ is now a proper transformation, and obtaining the corresponding Euler angles, $\mathbf{R}_{1R}$ = (0.000, 15.61, −90.00), results in an identical hf-tensor in the molecular frame. This orientation is depicted in Figure 5 lower, where the component A_{yy} = −69.24 G of the F(1)-hf interaction is seen.

The hf Tensors in the Principal Frame. $\mathbf{A}(^{13}C)$ = (−24.368, −24.368, 48.737) + 264.18570 Gauss = (239.82, 239.82, 312.92) Gauss. $\mathbf{A}(^{19}F)$ = (−72.955, −69.244, 142.199) + 138.32457 Gauss = (65.369, 69.080, 280.523) Gauss.

For the carbon, the tensor is diagonal in the molecular frame.

$$\mathbf{A}(^{13}C) = \begin{pmatrix} -24.368 & 0.000 & 0.000 \\ 0.000 & -24.368 & 0.000 \\ 0.000 & 0.000 & 48.737 \end{pmatrix} \text{Gauss}$$

Eulers $\mathbf{R}(^{13}C)$ = (3.45, 0.00, 0.00) degrees.

The hf parameters for the fluorine atoms are as follows:

$$\mathbf{A}_1 = \begin{pmatrix} 69.08 & 0.000 & 0.000 \\ 0.000 & 80.933 & -55.741 \\ 0.000 & -55.741 & 264.93 \end{pmatrix} \text{Gauss}$$

Eulers $\mathbf{R}_1$ = (180.0, 164.4, −90.00) degrees.

Notice that the value 164.4 of the above beta Euler angle agrees, in the sense of 180−164.4 = 15.6°, with the beta of the following two fluorine atoms.

DOI: 10.1021/acs.jpca.5b05648
J. Phys. Chem. A 2015, 119, 9385−9404

$$\mathbf{A}_2 = \begin{pmatrix} 77.978 & 5.1357 & 48.280 \\ 5.1357 & 72.040 & 27.870 \\ 48.280 & 27.870 & 264.93 \end{pmatrix} \text{Gauss}$$

Eulers $\mathbf{R}_2$ = (179.99, 15.61, 150.0) degrees.

$$\mathbf{A}_3 = \begin{pmatrix} 77.978 & -5.1357 & -48.280 \\ -5.1357 & 72.040 & 27.870 \\ -48.280 & 27.870 & 264.93 \end{pmatrix} \text{Gauss}$$

Eulers $\mathbf{R}_3$ = (0.00508, 15.61332, 29.995) degrees.

An EPR simulation of the rigid CF_3 is shown in Figure 6. The *EasySpin* software was employed using the above calculated

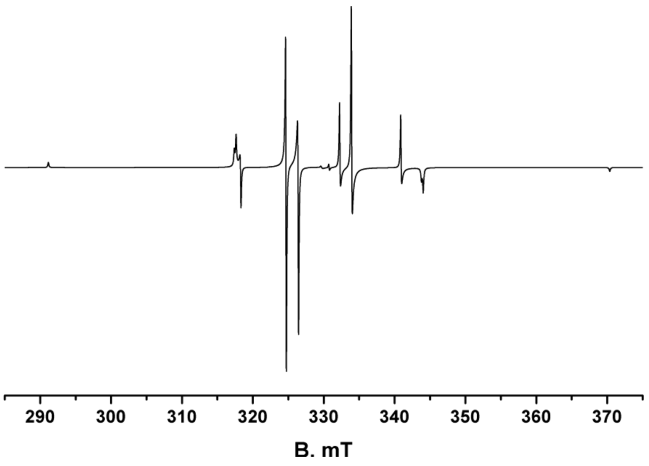

Figure 6. *EasySpin* simulation of the EPR spectrum of the CF_3 radical using the parameters computed by the Gaussian and averaging the dipolar interaction tensors of the three fluorine nuclei in the molecular frame proposed in this work resulting in the totally symmetric *A*-quartet of the $\mathbf{C}_3$ system. Axial symmetry and the exact high-temperature simulation accounted by the calculated parameters $A_\perp$ = 75 G, $A_\parallel$ = 264 G, $g_\perp$ = 2.004244, $g_\parallel$ = 2.001664, and f_{res} = 9.27 GHz was employed. The individual lines were assumed to be 0.1 mT wide Lorentzians. The superimposed doublet was assumed to possess the same parameters as the quartet.

axially symmetric **g**-tensor and an axially symmetric **A**-tensor obtained as the arithmetic mean of the above $\mathbf{A}_1$, $\mathbf{A}_2$, and $\mathbf{A}_3$ results; see Table 4. The quartet and one doublet with the same EPR parameters and the same integral intensities are superimposed in the figure.

The same result as the simulation in Figure 6 was obtained by summing the individual hf proton tensors in the molecular frame. This corresponds using only an *A*-quartet and a doublet, disregarding the reduced symmetry of the *E*-doublets.

The complete polycrystalline spectrum by Maruani et al.[8] Figure 3, of the original paper, was calculated with c^x = 87 G, c^y = 80 G, c^z = 263.5 G, and a line width of 7 G. In simulating the EPR spectrum of the CF_3 radical, Maruani et al. took, indeed, $g_\perp$ = 2.0042, $g_\parallel$ = 2.0024 after Rogers and Kispert.[19] When trying the axial symmetry of the hf tensor, Maruani et al.[8] used the effective value of the hyperfine coupling tensors parallel to the symmetry axis: $c_e^\parallel$ = 252.2 G. The angle between the molecular symmetry axis and the plane perpendicular to each C−F bond equals to 17.8°. Our computed value is ca. 16 degrees; see the above Euler angles $\mathbf{R}_1$, $\mathbf{R}_2$, and $\mathbf{R}_3$; e.g., for the $\mathbf{R}_1 = (\alpha_1, \beta_1, \gamma_1)$, observe that the β_1 = 164.4 gives 180 − β_1 = 15.6°. They relate this value to the actual principal values of the hyperfine coupling tensors for the fluorine atoms. Thus, $c_e^\parallel$ = 252.2 G and a = 143.4 G bring about $c^x = c^y$ = 83.35 G and c^z = 263.5 G. In computing the axially symmetrical spectrum, the authors also tried a line width equal to 4 G.

Except for that those attempts, Figure 6 is not giving identical lineshapes to the experimental results for matrix-isolated CF_3. It will be shown further that just summing analytically and averaging the three proton tensors in the molecular frame is valid only for planar molecules. In fact this is a good way to examine the planarity of similar systems. On the other hand the experimental spectra differ significantly in the transitions next to the outer ones, which are much more intense than the simulated.

In comparing the calculated EPR spectrum of the rigid CF_3 using vacuum DFT magnetic parameters to experiments of trapped radicals, one has to account for effects which may contribute essentially to their differences.

One of them is the matrix shifts, studied by Dmitriev and Benetis,[20] of both the **g**- and **A**-tensors which are, possibly, more pronounced for the pyramidal CF_3 molecule compared to the plane CH_3 molecule. The second is the rotational effect on the EPR parameters. Indeed, Maruani et al.[8] found a large temperature effect on the EPR lineshape of the CF_3 in solid Kr, which was readily noticed already at as a low sample temperature as 10 K.

Symmetrization. A theoretical attempt will be made to compute analytically the hf tensors that correspond to the single electron from the spin Hamiltonian, rearranging them to a quartet and a two doublets in agreement with the basic $\mathbf{C}_3$ symmetry of the CX_3 species, with spin I = 1/2 for the X-nucleus (H, F).

The numerical computation of the powder EPR considers the three hf interactions and averages over all the orientations of the corresponding tensors separately. The difference is that, while we only need to simply superimpose the hf couplings of the symmetry determined coupled representation interactions, the numerical simulation of the *EasySpin* considers the successive splitting of the electron resonance by convoluting the three hf- coupled proton spectra one after the other.

By the present method, one gains both an important simplification for the EPR lineshape computation by immediately plotting the basic quartet and an important geometrical characterization of the XY_3 radical systems isolated in low temperature inert matrices. Namely, eventual diagonal and axial doublets in certain systems may indicate planar XY_3 radicals.

Next is presented a comparison of EPR lineshape powder simulations with the general numerical averaging vs a superposition of the smaller pieces, a diagonal quarter and two doublets, of the problem. Eventual theoretical development of this part could even lead to a fully analytical solution of the powder lineshape

The hf Spin Hamiltonian in the Coupled Nuclear C_3 Representation. Starting with the total spin Hamiltonian for methyl type radicals,

$$H = \beta \mathbf{B}\cdot\mathbf{g}\cdot\mathbf{S} + \mathbf{S}\cdot\sum_{i=1}^{3}\mathbf{A}_i\cdot\mathbf{I}_i - g_N\beta_N\mathbf{B}\cdot\sum_{i=1}^{3}\mathbf{I}_i \qquad (3)$$

The nuclear sum in the hf part of it,

$$\mathbf{V}(\text{hf}) = \sum_{i=1}^{3}\mathbf{A}_i\cdot\mathbf{I}_i$$

DOI: 10.1021/acs.jpca.5b05648
J. Phys. Chem. A 2015, 119, 9385−9404

is singled out attempting to symmetrize it within the minimal $\mathbf{C}_3$ group of the CH_3 and CF_3 molecules.

The following *ansatz* entails a quartet $\mathbf{Q}$ hf interaction and two doublets $\mathbf{D}^{(1)}$ and $\mathbf{D}^{(2)}$ and the corresponding operators $\mathbf{F}$ of the nuclear spin in the coupled representation.

$$\begin{aligned}\mathbf{V}(\mathrm{hf}) &= \mathbf{A}_1\cdot\mathbf{I}_1 + \mathbf{A}_2\cdot\mathbf{I}_2 + \mathbf{A}_3\cdot\mathbf{I}_3 \\ &= \mathbf{Q}\cdot\mathbf{F}^{(A)}(3/2) + \mathbf{D}^{(1)}\cdot\mathbf{F}^{(E_+)}(1/2) + \mathbf{D}^{(2)}\cdot\mathbf{F}^{(E_-)}(1/2)\end{aligned} \tag{4}$$

It is based in the symmetry reduction of the full rotation group involving the irreducible *A* and *E* representations within the $\mathbf{C}_3$ group.

The result thus being, see Supporting Information (SI) section S1,

$$\mathbf{Q} = \frac{1}{3}(\mathbf{A}_1 + \mathbf{A}_2 + \mathbf{A}_3) \tag{5a}$$

$$\mathbf{D}'^{(1)} = \frac{1}{3}[(\mathbf{A}_1 - \mathbf{A}_2) - \varepsilon^*(\mathbf{A}_2 - \mathbf{A}_3)] \tag{5b}$$

$$\mathbf{D}'^{(2)} = \frac{1}{3}[(\mathbf{A}_1 - \mathbf{A}_2) - \varepsilon(\mathbf{A}_2 - \mathbf{A}_3)] \tag{5c}$$

where the variable $\varepsilon = \exp(i2\pi/3)$ is related to the period $2\pi/3$ of the C_3 rotation.

It is obvious that by introducing the quartet we recognize the sum of the three hf-proton tensors in the molecular frame. However, two additional complex doublets for the minimum $\mathbf{C}_3$ symmetry are found, for both CH_3 and CF_3. Two are the possible ways to avoid complex arithmetic: either use real combinations of the *E*-states or go over to the $\mathbf{D}_3/\mathbf{C}_{3v}$ groups that have real characters. Both attempts give comparable results as seen in SI, section S1.

It is observed that the above two doublet matrices are complex conjugates.

Therefore, if they are added, actually averaged, a real doublet, which in the CH_3 is in addition diagonal in the molecular frame, is obtained. The other doublet is the imaginary part of their combination.

The corresponding doublet for the CH_3 on the other hand exchanges only the *x*- and *y*-axes! For the significance of this observation, see further.

The diagonal isotropic Fermi contact part was added afterward. The first doublet in the CH_3 case was as seen diagonal in the molecular frame. Thus, the planarity is related to the diagonal form of the hf tensor of the doublets, at least one of them. The fact that the doublets may not be diagonal in the molecular frame indicates that they are of the not totally symmetric *E*-representation.

A computation of the quartet and the two doublets within the $\mathbf{C}_{3v}$ (pyramidal) and $\mathbf{D}_3$ (planar) symmetry results to the Hamiltonian following real nuclear multiplets in the coupled representation.

$$\begin{cases} \mathbf{Q} = \frac{1}{3}(\mathbf{A}_1 + \mathbf{A}_2 + \mathbf{A}_3) \\ \mathbf{D}_1 = \frac{1}{3}(\mathbf{A}_1 + \mathbf{A}_2 - 2\mathbf{A}_3) \\ \mathbf{D}_2 = \frac{1}{\sqrt{3}}(\mathbf{A}_1 - \mathbf{A}_2) \end{cases}$$

In Supporting Information, section S1, the derivation of these multiplets are given along with the corresponding $\mathbf{C}_3$ results.

Simulation CH_3 EPR Using C_3/D_3 Multiplets. Using the computed hyperfine tensors $\mathbf{A}_1$, $\mathbf{A}_2$, and $\mathbf{A}_3$ for the three protons of CH_3 in Gauss units presented in the above quantum chemistry section and applying MATHEMATICA, the following final real doublets were obtained except for the usual quartet $\mathbf{Q}$ obtained by summation of the proton hf tensors in the molecular frame.

Both hf's for the quartet and the first doublet of the CH_3 further down are very close to diagonal form, indicating geometry close to planar.

The eigenvalues/diagonal of the quartet $\mathbf{Q}$ are (−23.2577, −23.257, −22.313) Gauss, which actually do display axial symmetry and relatively small, ca. 1 G, overall anisotropy.

The first doublet $\mathbf{D}_1$ has eigenvalues (−30.0163, −16.0237, −23.1352) Gauss and is diagonal, while the second doublet $\mathbf{D}_2$ has eigenvalues (−30.016, −16.0234, −23.0197) Gauss, differing only slightly from the first one, but with orientation differing significantly from the quartet.

In detail, the hf matrix for the first doublet in the molecular frame is:

$$\mathbf{D}_1 = \begin{pmatrix} -30.0163 & 0.000 & 0.000 \\ 0.000 & -16.0237 & -0.00932177 \\ 0.000 & -0.00932177 & -23.1352 \end{pmatrix}$$

This doublet does not need diagonalization.

The second doublet spin Hamiltonian matrix in the molecular frame is:

$$\mathbf{D}_2 = \begin{pmatrix} -23.0197 & 6.9963 & 0.00894609 \\ 6.9963 & -23.0197 & 0.000 \\ 0.00894609 & 0.000 & -23.0197 \end{pmatrix}$$

and has eigenvalues (−30.016, −16.0234, −23.0197) Gauss, and eigenvectors,

$$\mathbf{R}(\mathbf{D}_2) = \begin{pmatrix} -0.707107 & 0.707106 & 0.000904169 \\ -0.707107 & -0.707106 & -0.000904169 \\ 0.000 & -0.00127869 & 0.999999 \end{pmatrix}$$

or equivalently the Euler angles $\mathbf{R}_2$ = (−45.00, 0.00, −90.00) degrees.

Both the hf doublets are thus given above in the plane of the molecule.

It looks like here that the two doublets are very close to each other and differ from the quartet.

Less trivial is the CF_3 case, where also both doublets are not diagonal.

Employing the *EasySpin* software, we simulated the CH_3 spectra in Figure 7. In the simulation of the quartet is seen that the outer lines display an extra splitting due to the small anisotropy of the hf interaction quartet tensor.

We further simulate in Figure 8 the spectra of the two $E^{\pm}$-doublets, which are very similar to each other. They should not contribute to the EPR spectrum of the CH_3 quantum rotor at very low temperatures. However, they are superimposed in equal intensity to the quartet for higher temperatures. Once more it is indicated that the apparent spectral anisotropy should be very small at the lowest temperatures as the quartet hf

DOI: 10.1021/acs.jpca.5b05648
J. Phys. Chem. A 2015, 119, 9385−9404

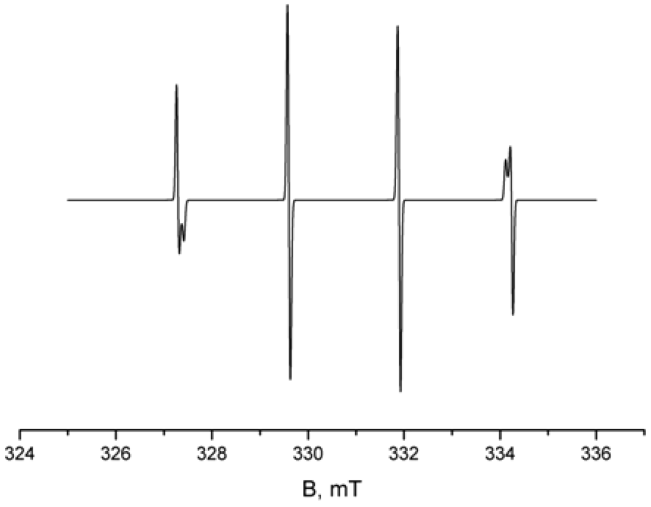

Figure 7. Simulation of the quartet EPR lineshape for the CH_3 radical. Parameters: A_{xx} = −23.2577 G, A_{xy} = 0, A_{xz} = 0, A_{yy} = −23.257 G, A_{yz} = 0.000053, A_{zz} = −22.313 G, isotropic g-factor =2.002320, Gaussian individual line width ΔH = 0.05 mT, microwave resonance frequency, f_{res} = 9.27 GHz.

interaction has almost equal Cartesian parallel and perpendicular components.

A superposition of the quartet and two doublets, Figure 7 and Figure 8, is shown in Figure 9.

The three different multiplets are normalized so that the quartet intensity equals to the sum intensities of the two doublets. One could believe that the intensity of the quartet should equal to the intensity of each doublet. However, at high temperatures, the hf multiplet sequence is 1:3:3:1. At those temperatures the two doublets sum up to give a doublet with integral intensity equal to the integral intensity of the quartet. As a result, the net integral intensity of the two initial doublets must equal to that of the quartet.

On the other hand, the computed A_{xx} = −30 G component in Figure 8, is smaller than the experimentally determined A_{yy}^{exp} = −34 G in N_2O and −38 G in CO_2, respectively. The experimental A_{xx}^{exp} = −14.7 G splitting, fairly well matches the computed A_{yy} = −16.1 G. Further adjustment to the parameters of the experimental N_2O spectra may be necessary. It seems, e.g., that a smaller splitting related to the calculated −9.8 G also emerges in the spectra. We actually found the third doublet with the components separated by 8.9 G which is close to the calculated 9.8 G; see the experimental spectra in Figures 10 and 11. Further details about the latter doublet are found in Supporting Information (SI), section S2.

The lineshape of Figure 9 will be compared to Figure 10 and Figure 11 where the experimental powder spectra of CH_3 in the N_2O and CO_2 solid matrices are reproduced. Evidently the "stopped" radical presented in Figure 9, restricted within the matrix cage, cannot be considered completely motionless since otherwise it violates the Heisenberg uncertainty principle. It is assumed that it performs small angle libration, a kind of motion also coupled to the total nuclear spin function through the symmetry requirements of the overall molecular wave function, as seen in Correnti et al.[5]

The simulation in Figure 10 is intended to explore how close to the experimental is the theoretical lineshape, when the **g**-tensor anisotropy and the line broadening are taken into account. The simulation was based on the above derivation of the quartet and doublets from the DFT computed **A**-tensors but adopting the isotropic g-value from the experimental axially symmetric **g**-tensor: $g_\perp$ = 2.00267 and $g_\parallel$ = 2.00229. Gaussian lineshape with line width set to 0.1 mT, and microwave frequency equal to 9.391 GHz were assumed. The relative intensities of the doublets and the quartet were also adjusted to simulate the experimental relative intensities.

Thus, the experimental results support the theoretically obtained hf interaction parameters of the CH_3 radical, represented by a sum of the A-symmetry quartet and two E-symmetry doublets. Also, the present theory explains the weak additional resonances in the EPR spectrum of CH_3 in N_2O and CO_2 matrices, and on the silica gel surface (Benetis and Dmitriev[21]).

As the sample temperature is increased, the small amplitude transitions (doublets) in the above figure disappeared, while the J = 1 axially symmetric E-doublet superimposed on the two inner quartet lines got stronger. See the spectra below and the relevant discussion in Benetis and Dmitriev.[21]

The effects of rotation are further discussed in greater detail.

A similar as the above simulation but within the $\mathbf{D}_3$ symmetry which contains all the transformations of a planar radical species is given further. As seen it compares better to the experimental data in Figures 10 and 11.

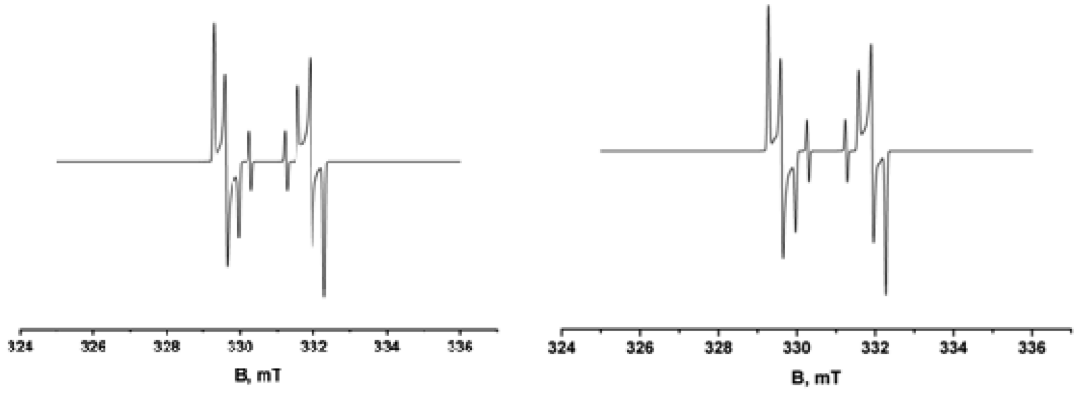

Figure 8. Left panel: Simulation of the first doublet $\mathbf{D}_1$. The parameters used are: A_{xx} = −30.0163 G, A_{xy} = 0, A_{xz} = 0, A_{yy} = −16.0237 G, A_{yz} = −0.009321977, A_{zz} = −23.1352 G. Right panel: Simulation of the second doublet $\mathbf{D}_2$. The parameters used A_{xx} = −23.0197 G, A_{xy} = 6.9963, A_{xz} = 0.00894609, A_{yy} = −23.0197 G, A_{yz} = 0, A_{zz} = −23.0197 G. The width ΔH = 0.05 mT is taken, the same as in the quartet. The isotropic g-factor = 2.002320 and microwave resonance frequency, f_{res} = 9.27 GHz, are assumed.

DOI: 10.1021/acs.jpca.5b05648
J. Phys. Chem. A 2015, 119, 9385−9404

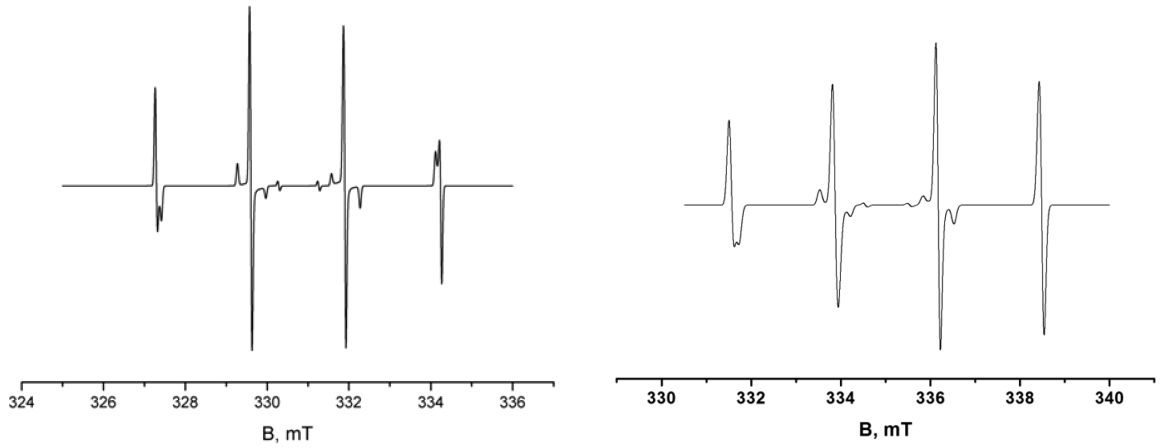

Figure 9. Left panel: The simulated spectrum obtained as a superposition of the quartet, Figure 7, and two doublets, Figure 8. The total integral intensity of doublets is equal to the integral intensity of the quartet. Right panel: Spectrum obtained for the same parameters except for adopting axially symmetric **g**-tensor, $g_{\perp} = 2.00267$ and $g_{\parallel} = 2.00229$, and relative intensities of the quartet and doublets picked to bring the simulation closer to the experimental CH_3 EPR in N_2O matrix. The resonance frequency was set to $f_{res} = 9391$ MHz. This spectrum resembles the experimental spectra of methyl radical in solid N_2O and CO_2 with the contribution of the nonrotating[21] CH_3. In that case we may assume that the radical performs librations.

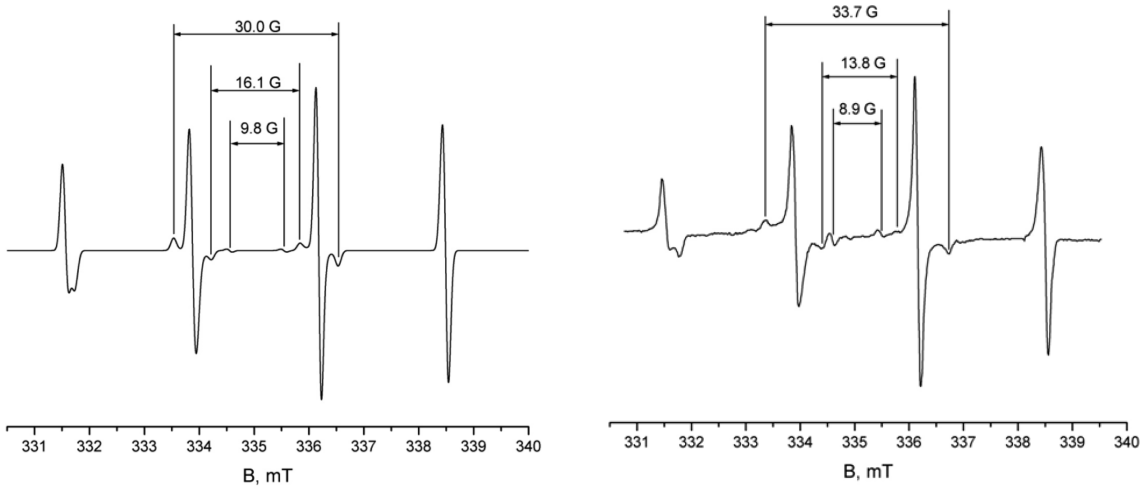

Figure 10. Left panel: Simulated EPR spectrum of CH_3 in solid N_2O for the $\mathbf{C}_3$ − symmetry hf parameters. The microwave resonance frequency was $f_{res} = 9391$ MHz. The spectrum was obtained after Figure 9, except that (i) axially symmetric **g**-tensor was used and (ii) the lines were broadened after the superhyperfine interaction was taken into account. Right panel: Experimental EPR spectrum of the CH_3 radical trapped in solid N_2O. Microwave resonance frequency, $f_{res} = 9391$ MHz. The sample temperature during recording was 8.7 K. The substrate temperature during deposition was 17 K.

Apart the simulation in Figure 10, one could see only two small intensity doublets in the spectrum of Figure 12, the second one being split by 8.3 G which is close to the smallest 8.9 G splitting for CH_3 in N_2O. Figure 13 simulates experimental CH_3 spectra obtained in N_2O and CO_2 matrices. Only the N_2O matrix is mentioned in the figure caption of Figure 13 since the **g**-tensor components are selected to fit the simulation of the N_2O experiment. However, the radical simulation in vacuum is performed, and therefore, the result is applicable for comparison between these two matrices. The 37.0 G splitting nearly coincides with the largest 38 G doublet splitting observed for CH_3 in CO_2.

Higher than C_3, Planar D_3 Symmetry. While that quartet was identical as in the $\mathbf{C}_3$ symmetry, the new $\mathbf{D}_3$ doublets used were given by

$$\mathbf{D}_1 = \begin{pmatrix} -30.0163 & 12.118 & 0.0154951 \\ 12.118 & -16.0237 & -0.00932177 \\ 0.0154951 & -0.00932177 & -23.1352 \end{pmatrix}$$

(left-handed)

Eigenvalues = (−37.0126, −9.02738, −23.1351) Gauss

eigenvectors

$$= \begin{pmatrix} -0.866025 & 0.5000 & 0.00130283 \\ 0.5000 & 0.866025 & -0.00002306 \\ 0.00113982 & -0.000631444 & 0.999999 \end{pmatrix}$$

Eulers $\mathbf{R}(\mathbf{D}_1)$ = (178.99, 179.92, 28.99) degrees

DOI: 10.1021/acs.jpca.5b05648
J. Phys. Chem. A 2015, 119, 9385−9404

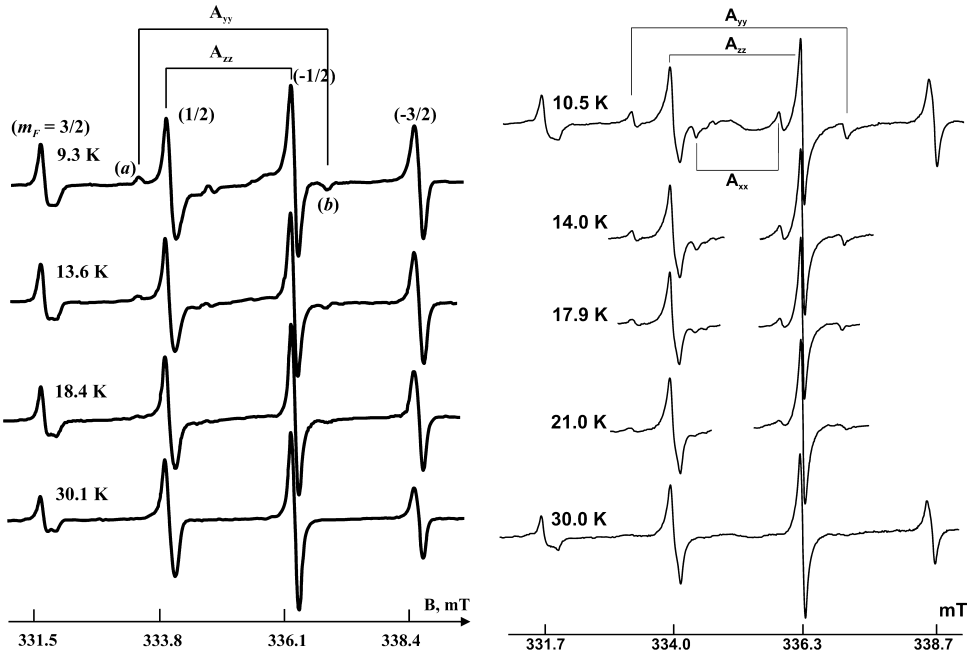

Figure 11. Left panel: CH_3 in solid N_2O, $A_{yy} = -34.0$ G. Right panel: CH_3 in solid CO_2. $A_{xx} = -14.7$ G, $A_{yy} = -38.3$ G. In both spectra, the A_{zz} pair of weak lines turned out to be unresolved because it was superimposed on the two much stronger central axially symmetric transitions. Hence, we estimate $A_{zz} \approx 23$ G.

$$\mathbf{D}_2 = \begin{pmatrix} -35.1382 & -6.9963 & -0.00894609 \\ -6.9963 & -10.9023 & -0.0161458 \\ -0.00894609 & -0.0161458 & -23.2197 \end{pmatrix}$$

Eigenvalues = (−37.0122, −9.0276, −23.2197) Gauss

eigenvectors

$$= \begin{pmatrix} -0.965925 & -0.258819 & -0.000929455 \\ -0.258818 & 0.965926 & -0.000935747 \\ -0.00113997 & 0.000663302 & 0.999999 \end{pmatrix}$$

Eulers $\mathbf{R}(\mathbf{D}_2)$ = (45.19, 179.91, −149.81) degrees.

The above Euler angles show that both doublets are practically in the plane of the radical.

Simulation of CF_3 EPR Using C_3/C_{3v} Multiplets. The hf interaction tensors $\mathbf{A}_1$, $\mathbf{A}_2$, and $\mathbf{A}_3$, of the three fluorine atoms of the CF_3 radical with the unpaired electron, respectively, in Gauss were given in the above computational quantum chemistry section.

The hf matrix for the quartet ($F = 3/2$) in the molecular frame is, in Gauss,

$$\mathbf{Q} = \begin{pmatrix} 75.012 & 0.000 & 0.000 \\ 0.000 & 75.0044 & 0.00005 \\ 0.000 & 0.0000533 & 264.934 \end{pmatrix}$$

where obviously the eigenvanlues are (75.012, 75.0044, 264.934) Gauss, as is seen in the simulation of Figure 14. The quartet here, as in methyl, is found to be axial conforming to the axial symmetry of the pyramidal C_3/C_{3v} species. However, in this case compared to methyl, the parallel z-component deviates strongly from the perpendicular hf components, giving strong axial anisotropy characteristics to the spectrum.

The aim of the present theory was primarily the powder spectra simulation of radical species of the simple C_3 symmetry with quenched motion. Instead of considering separately the hf couplings of the three protons with the symmetry related principal axes in, e.g., CH_3, the hf coupling from the electron point of view was considered. It is just a rewriting of a static spin Hamiltonian using the coupled nuclear spin representation within the C_3 symmetry and the superposition of the corresponding EPR lineshapes, assuming temperature determined probabilities for the classical rotational conditions for CF_3, see Tables 1 and 3.

However, paying special attention to the doublets that deal with the excited rotational states, always active for CF_3, the simulation in Figure 15, was performed.

In Figure 15, a comparison of the theoretical C_{3v} EPR spectra of CF_3 is given with the experimental spectra by Maruani et al.[8] Although the new C_{3v} result is closer to the Maruani's experiment, obviously, some part of the new theory is still inadequate to retrieve the exact experimental results for CF_3.

The improvement of this part of the theory is currently in progress and is going to lead to simpler and less time-consuming powder simulation than the straightforward successive splitting of the electron resonance by the three protons. Additional spectral defects depend on the inaccuracy of the theoretically computed values of the parameters.

It seems, e.g., that the 75 G component of the quartet tensor is somewhat smaller. An attempt to involve the **g**-tensor anisotropy did not help as seen in Figure 15 in spite of some additional improvements of the symmetry applied in the parameters computation.

Higher than C_3, Pyramidal C_{3v} Symmetry. The parameters used in the simulations of Figures 15 and 16c were the same as above for the quartet, while the doublets were found to be as following within the C_{3v} group.

$$\mathbf{D}_1 = \begin{pmatrix} 135.359 & 5.13574 & 48.2798 \\ 5.13574 & 141.289 & -27.8704 \\ 48.2798 & -27.8704 & 138.324 \end{pmatrix} \text{(left-handed)}$$

DOI: 10.1021/acs.jpca.5b05648
J. Phys. Chem. A 2015, 119, 9385−9404

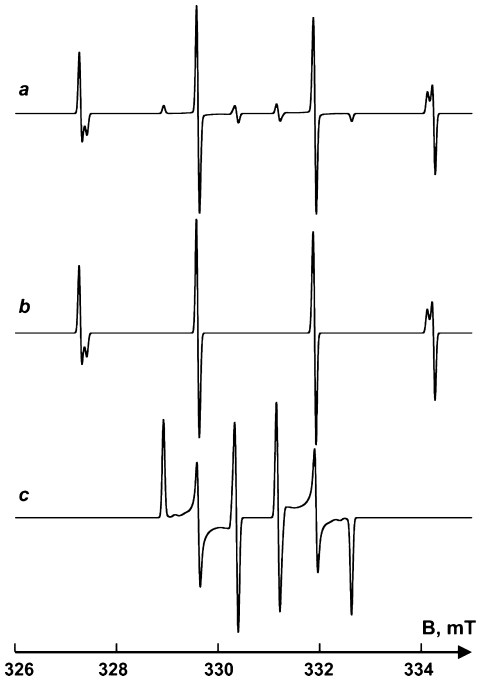

Figure 12. Simulation of the EPR spectrum of the CH_3 radical within the D_3 symmetry. The **g**- tensor was assumed to be isotropic. (a) Superposition of the quartet and two doublets. (b) The quartet. (c) The doublet 1. The two doublets yielded nearly identical simulated powders. The quartet parameters were kept the same as above. Doublet 1: A_{xx} = −30.0163 G, A_{xy} = 12.118 G, A_{xz} = 0.0154951 G, A_{yy} = −16.0237 G, A_{yz} = −0.00932177 G, A_{zz} = −23.1352 G. Doublet 2: The parameters used are A_{xx} = −35.1382 G, A_{xy} = −6.9963 G, A_{xz} = −0.00894609 G, A_{yy} = −10.9023 G, A_{yz} = −0.0161458 G, A_{zz} = −23.2197 G. The isotropic *g*-factor was 2.002320, while Gaussian 0.5 G wide lineshapes were applied to the individual transitions. The microwave resonance frequency was f_{res} = 9.27 GHz. The three different multiplets were normalized so that the quartet intensity was equal to the sum intensities of the two doublets.

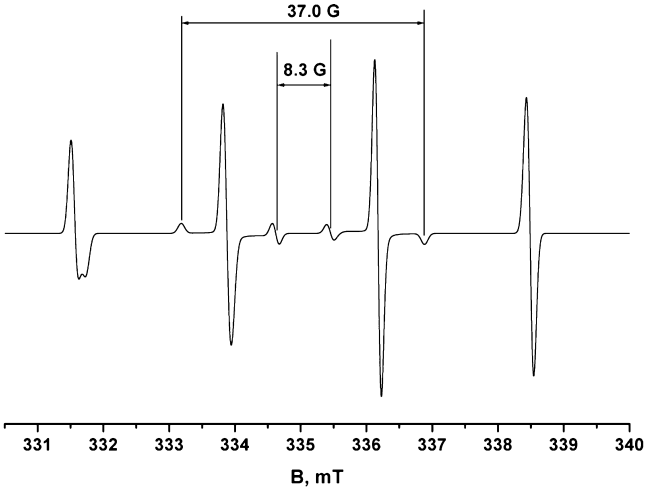

Figure 13. Simulated EPR spectrum of CH_3 in solid N_2O. The microwave resonance frequency was f_{res} = 9391 MHz. The spectrum was obtained after Figure 12a, except that in addition, the axially symmetric **g**-tensor: $g_\perp$ = 2.00267 and $g_\parallel$ = 2.00229 was assumed. Also, additional line broadening by the assumed superhyperfine interaction was added through Gaussian line width 0.1 mT. The relative intensities of the doublets and the quartet were changed to match the experimental relative intensities.

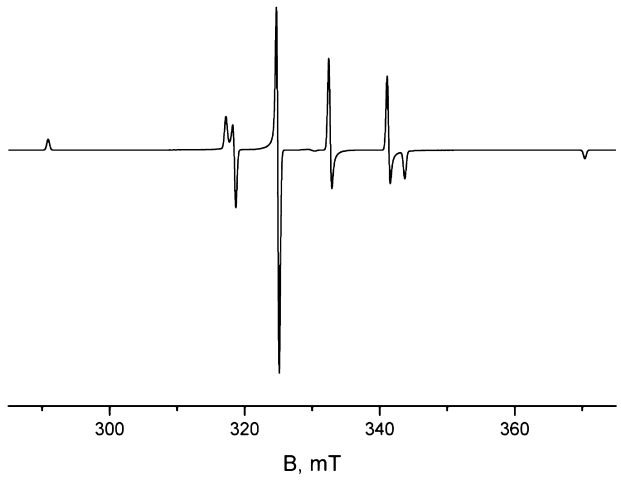

Figure 14. Totally symmetric *A*-quartet of the rigid CF_3 radical. The EPR parameters: A_{xx} = 75.012 G, A_{xy} = 0, A_{xz} = 0, A_{yy} = 75.044 G, A_{yz} = 0.00005 G, A_{zz} = 264.934 G; isotropic *g* − factor =2.002320; Gaussian individual line width ΔH = 0.4 mT; microwave resonance frequency, f_{res} = 9.27 GHz. Exact diagonalization was applied in the spectral simulation.

$$\mathbf{D}_2 = \begin{pmatrix} 133.187 & -2.96512 & -27.8744 \\ -2.96512 & 143.459 & -48.273 \\ -27.8744 & -48.273 & 138.324 \end{pmatrix}$$

To check the *EasySpin* for the possibility of two **A**-tensors attributed to one molecule, the spectrum of the doublets were considered through a system of one electron coupled to the two fluorine nuclei with the **g**- and **A**-tensors using the calculated $\mathbf{D}_1$ and $\mathbf{D}_2$ doublets. In Figure 15b is shown the spectrum of the two doublets, and finally in Figure 15c the superposition of the two doublets with the quartet is shown rendering an improved CF_3 EPR lineshape simulation. This way to handle with the problem of non planar radicals is currently under further consideration and will be presented in our next work. The hypothesis is that, at low temperatures, the heavy trifluoromethyl CF_3 radical rotational states are to be considered in the intermediate thermodynamical limit between (i) the nuclear spin coupled to the rotation states and (ii) considered separately. However, this does not apply to the much lighter protons of the CH_3 and SiH_3 radicals, which are strongly coupled to the radical rotation state.

For convenience we repeat the approximately diagonal quartet (75.012, 75.0044, 264.934) Gauss, and using the above two doublets $\mathbf{D}_1$ and $\mathbf{D}_2$ in Gauss, as they were computed earlier in this section:

A general *EasySpin* simulation of the experimental spectra is given in Figure 16a, where a numerically simulated powder spectrum for rigid CF_3, considers explicitly the separate hf interactions of the three fluorine ^{19}F nuclei, with the corresponding symmetry related principal axes for each of them.

For convenient comparison of the simulations, we provide in Figure 16 the spectra obtained for the CF_3 radical in rigid state with symmetry-related principal axes of the three ^{19}F; see Figure 15. The spectra were generated using a free *EasySpin* example "trifluoromethyl; CF_3 radical in gas matrix at low temperature". In this example, the method of calculation was chosen as the second-order perturbation and further changing

DOI: 10.1021/acs.jpca.5b05648
J. Phys. Chem. A 2015, 119, 9385−9404

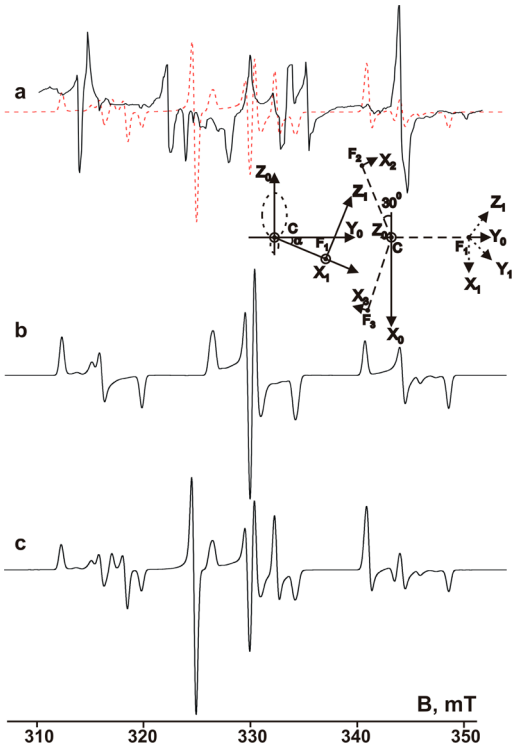

Figure 15. (a) Simulation of the rigid CF_3 within the C_3 group (b and c) compared to Maruani's result (a). Only the central part of the spectrum is shown. The spectrum in red is the simulation with the conditions described in b and c below, while that in black is the Maruani's experiment. Unfortunately, the correspondence between the simulation and experiment is not well. The situation cannot be improved by the line width change. (b) Two doublets simulated through a system of one electron coupled to the two fluorine atoms with equal **g**-tensor and different **A**-tensors. The computed **A**-tensors of the $\mathbf{D}_1$ and $\mathbf{D}_2$ doublets were shown above in this section. The g-tensor was taken as $\mathbf{g}$ = (2.0042442, 2.0042458, 2.0016636) as it was also computed in the section about the trifluoromethyl CF_3 radical section. The individual lines are Gaussian with width equal 0.4 mT. (c) Superposition of the two doublets and one quartet, with the computed hf values given in this section.

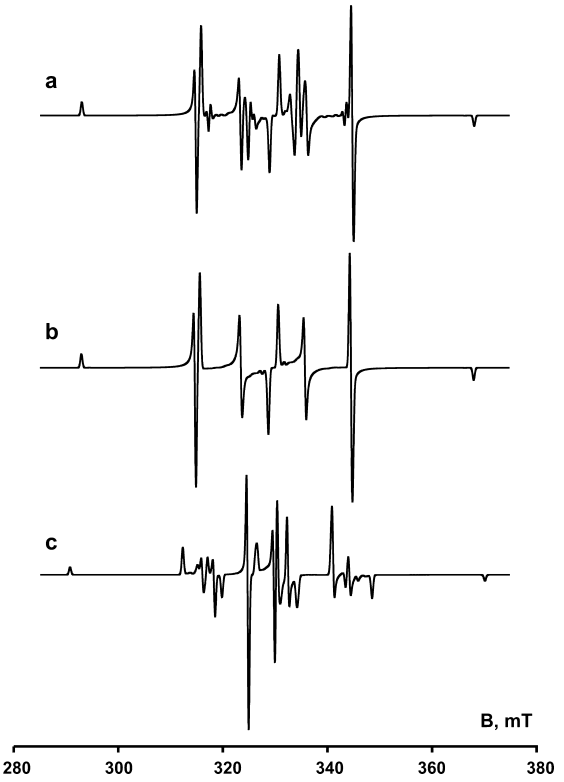

Figure 16. (a) Exact computation for the CF_3 for randomly oriented radicals by the *EasySpin* software. Each ^{19}F nucleus has hf principal value A_{xx} = 80 G, A_{yy} = 87 G, A_{zz} = 262 G, and axially symmetric **g**-tensor in the molecular frame (the parallel-direction along the 3-fold symmetry axis), $g_{\parallel}$ = 2.0024, $g_{\perp}$ = 2.0042. The individual line is Gaussian of 4 G width. The microwave resonance frequency was 9.27 GHz. "*A*" principal angles: (0, β, 0), (0, β, $2\pi/3$), (0, β, $-2\pi/3$), where $\beta = -17.8°$, as it was suggested by Prof. Anders Lund.[22] (b) Second-order computation for the CF_3 radical with the same parameters as in (a) by the *EasySpin* software. Only the condition exact computation to second order approximation has been employed. (c) Superposition of the two combined doublets with the quartet in the wide scan mode.

the method by "matrix" to exact diagonalization.[22] The second-order computation is also given in Figure 16b for completeness.

EXPERIMENTAL SECTION

It is obvious from the qc- computations that the hf splitting for each proton in CH_3 radical is rhombic, as expected, Figure 1, but there are three protons and they are situated around the p_z-orbital symmetrically. This arrangement changes the situation for the electron spin, radically. The resulting cumulative hf tensor from the electron point of view should become overall axial. Indeed, the methyl radical is a rather symmetric molecule. The significance of that there is no need for rotational averaging, as it is regularly claimed in the literature, for that. The 3-fold symmetry for the **A**-tensor of the unpaired electron becomes clear from the result obtained when the proton tensors are summed up in the 3D space, in spite to the rhombic appearance of their **A**-tensors. The conventional superposition of the doublets in Figure 17 does not show this improvement.

The computed isotropic component, −22.95 G, seems to be somewhat smaller than the experimental for the freely rotating radical, −23.37 G, taken from both the article by Davis et al.,[23] and our estimate based on the data for matrix isolated methyl radical, Dmitriev and Benetis.[20] A more systematic comparison with experimental data available from the literature is discussed further. One should keep in mind that the present qc computations are performed for the radicals in vacuum. On the other hand, a more systematic computation series with different basis sets and quantum methods is outside the scope of the present work.

The parallel and perpendicular components of the **A**-tensor in vacuum were computed to $A_{\parallel}^{\text{theor}} = -22.32$ G and $A_{\perp}^{\text{theor}} = -23.27$ G, respectively. Thus, inequality $|A_{\parallel}^{\text{theor}}| < |A_{\perp}^{\text{theor}}|$ is in good agreement with our experimental data for CH_3 in solid gas matrices of linear molecules (Benetis and Dmitriev[21,24]).

Moreover, the experimental $A_{\perp}^{\text{exp}}$ values are slightly smaller compared to the theoretical, which may be explained by the matrix effect on the hyperfine coupling which becomes stronger for matrix isolation going from N_2 to CO_2 solids. However, the theoretical perpendicular component seems to be underestimated obtaining values smaller than the experimental ones. Accordingly, the theoretical isotropic coupling estimated as $A_{\text{iso}}^{\text{theor}} = [(A_{\parallel}^{\text{theor}} + 2A_{\perp}^{\text{theor}})/3] = -22.95$ G, is smaller compared to the values measured for the Ne, Ar, and H_2 matrices with the weakest radical−matrix interaction (see Table 5) and hence the smallest matrix shifts. Interestingly, the extent

DOI: 10.1021/acs.jpca.5b05648
J. Phys. Chem. A 2015, 119, 9385−9404

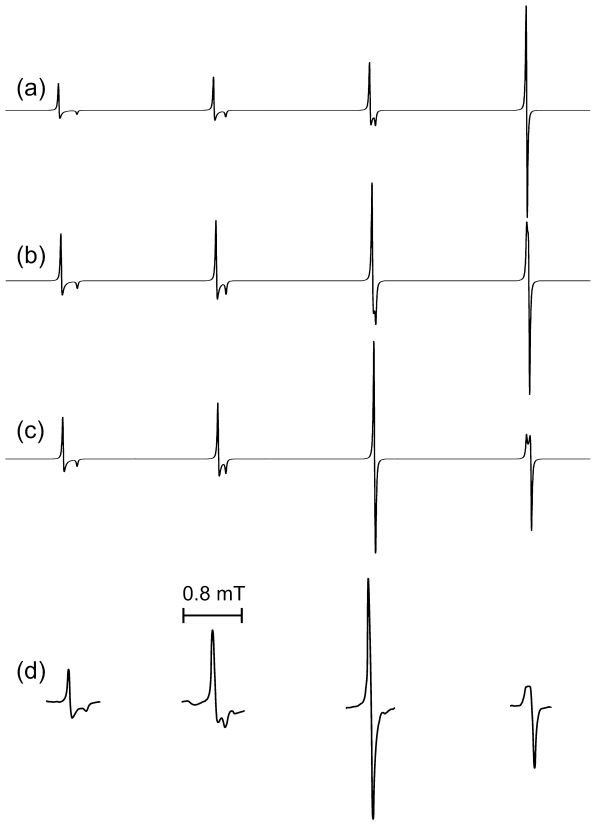

Figure 17. Simulated EPR spectrum of the methyl radical *A*-symmetry quartet. The figure shows the gradual change in the lineshape as the modulus of the matrix shift $|\delta g_\perp|$ increases. The EPR parameters used in the simulation are taken equal to the theoretically predicted values, i.e., (a) $\delta g_\perp = 0\%$. (b) $\delta g_\perp = -0.009\%$, while other parameters remain as before. (c) $\delta g_\perp = -0.018\%$, while other parameters still correspond to the computed values in vacuum. (d) Experimental spectrum, for CH_3 trapped in solid CO at 4.2 K, Dmitriev and Zhitnikov.[28] The Bruker *WinEPR* software was applied in the simulation.

of the **A**-tensor axial anisotropy for methyl radical in vacuum is estimated by Dmitriev et al.[24] to $\Delta A^{free} = A_\parallel - A_\perp = 1.49$ G. This is somewhat larger in modulus compared to the qc-computation $\Delta A^{free} = -22.320 - (-23.266) = 0.946$ G, which, again, underestimates $|A_\perp|$.

Note the negative ΔA in solid Ar and Kr and the positive Δg in Ar. The reason proposed in Dmitriev[25] was based on the fast radical rotation about the in-plane axes. The negative Δg in Kr was suggested to originate from matrix effect on the **g**-tensor components which is particularly large in solid Kr (Table 6). All of the other anisotropies are in general positive for the **A**-tensor and negative for the **g**-tensor, except for beryl matrix which, thereby, presents one of the challenging issues.

The theoretical **g**-tensor anisotropy, $\Delta g = g_\parallel - g_\perp = -7.62 \times 10^{-4}$, is of the same order as the experimental in Table 5, i.e., $|-4.93 \times 10^{-4}|$, for the mostly motionless CH_3 in CO_2 matrix. Accounting for the CH_3 librations in matrices would, evidently, bring closer the above two values. However, one should also study the matrix effect on the **g**- and **A**-tensor components, in particular if the matrix affects the $g_\parallel$ differently than $g_\perp$, and similarly differences of matrix effects on $A_\parallel$ compared to $A_\perp$. From the experimental data, this fact is more obvious with such matrices as solid Kr or Xe, having outer electrons weakly coupled with the nucleus.

Solid Gas Matrix Experiments. An experimental and a simulated spectrum of CF_3 are presented in Figure 15. The experimental spectrum was obtained by photolysis of CF_3I in a noble gas matrix[8,26] probably by McDowell et al. in Vancouver many years ago.[8] It would be interesting to record a new experimental spectrum, showing the outer transitions with overall distance ca. 80 mT that are missing (Figure 18). We are currently in process of completing this task.

It is also of great interest to assess the calculated methyl radical isotropic *g*-factor. One could see from the literature no consent about the isotropic *g*-factor of the CH_3 radical in various matrices. Evidently, the discrepancy owes to the inaccuracy in the magnetic field correction needed because of the fact that the NMR gage is shifted from the center of the magnet poles occupied by a microwave cavity.

Another way of obtaining accurate magnetic field is to record a spectrum of an EPR probe with exactly known *g*-factor simultaneously with the studied spectrum. However, it is not an easy task to find a probe with well-known *g*-factor to the fifth digit to be employed at such a low temperatures. Stesmans et al.[27] used $S = 1/2$ g (4.2 K) = 1.99869 Si:P marker sample. Table 7 presents some data on the *g*-factor of CH_3 in several solid gas matrices. For our experiments, the magnetic field was well calibrated using the electron cyclotron resonance line position in magnetic field equal to "*g*" = 1.99987(12).

We calibrated our magnetic field with two NMR probes: one in the center of the magnet poles and another in the shifted position standard to our experiments. In the calibration measurements, the microwave cavity was removed from the magnet. It turned out in further experiments that the electron cyclotron resonance line positions was at almost exactly "*g*" =

Table 5. Spin Hamiltonian Parameters for the *A*-Line Transition of the CH_3 Radical Trapped in Low Temperature Matrices[a]

	parameters							
matrix	$A_\perp$	$A_\parallel$	A_{iso}	ΔA	$g_\perp$	$g_\parallel$	g_{iso}	Δg (10^{-4})
Ne			2.333(5)					
Ar			2.313(5)					
Kr			2.300(5)					
H_2			2.324(7)					
N_2	2.350(2)	2.252(4)	2.317(5)	0.099(3)	2.00262(12)	2.00225(12)	2.00250(12)	3.70(25)
CO	2.343(5)	2.233(5)	2.306(7)	0.110(6)	2.00263(12)	2.00220(12)	2.00249(12)	4.14(25)
N_2O	2.333(4)	2.198(4)	2.288(4)	0.135(3)	2.00267(12)	2.00229(12)	2.00254(12)	3.84(42)
CO_2	2.339(6)	2.197(2)	2.292(4)	0.142(6)	2.00264(12)	2.00215(12)	2.00248(12)	4.93(30)

[a]The principal axes of the **A**- and **g**-tensors are assumed to coincide. The hyperfine splitting is measured in mT; $\Delta A = A_\parallel - A_\perp$ and $\Delta g = g_\parallel - g_\perp$. Each hfc component is represented by its modulus.

DOI: 10.1021/acs.jpca.5b05648
J. Phys. Chem. A 2015, 119, 9385−9404

Table 6. A- and g-Tensor Anisotropies in Various Solid Gas Matrices[a]

matrix	Ar	Kr	N_2	CO
(ΔA, Δg)	(-0.01, $+3 \times 10^{-5}$)[b]	(-0.016, -3×10^{-5})[c]	($+0.099$, -3.7×10^{-4})[d]	($+0.110$, -4.1×10^{-4})[d]
	(-0.021, $+3 \times 10^{-5}$)[c]		($+0.065$, -1×10^{-4})[e]	($+0.105$, -4×10^{-4})[e]
matrix	N_2O	CO_2	silica gel	zeolite
	($+0.135$, -3.8×10^{-4})[d]	($+0.142$, -4.9×10^{-4})[d]	($+0.07$, -3×10^{-4})[f]	($+0.11$, -4×10^{-4})[g]
		($+0.146$, -5×10^{-4})[e]		($+0.14$, -9×10^{-4})[g]
matrix	beryl	sodium acetate trihydrate		
	(-0.038, $+2.6 \times 10^{-4}$)[h]	($+0.07$, ---)[i]		

[a]Compare to the computed $\Delta A = +0.0946$ mT, $\Delta g = -7.62 \times 10^{-4}$ for the methyl in vacuum. $\Delta A = A_{\parallel} - A_{\perp}$, $\Delta g = g_{\parallel} - g_{\perp}$. [b]Popov et al.[37] [c]Dmitriev, Y. A. *Low Temp. Phys.* **2008**, *34*, 75−77. [d]Dmitriev et al.[24] [e]Kiljunen, T., et al. *J. Phys. Chem. A.* **2010**, *114*, 4770. [f]Shiga, T.; Lund, A. *J. Phys. Chem.* **1973**, *77*, 453. [g]Danilczuk, M. *Nukleonika* **2005**, *50*, S51. [h]Andersson, L. O. *Phys. Chem. Minerals* **2008**, 10.1007/s00269-008-0245-3. [i]Rogers, M. T.; Kispert, L. D. *J. Chem. Phys.* **1967**, *46*, 221−223.

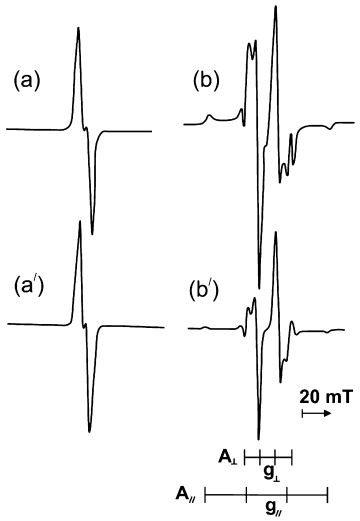

Figure 18. EPR spectrum of CF_3 radical in the complex $[(CF_3)_2CF]_2C^{\bullet}C_2F_5$ isolated in glassy matrix of hexafluoropropylene trimer measured at 77 by Allayarov et al.[29] The experimental spectra in (a′, b′) were simulated as were observed (a, a′) before and (b, b′) after 800 min UV photolysis at 77 K. The stick diagram of die CF_3 radical is shown in spectrum b′.

2.0000 which is expected for low density plasma. This result verifies the accuracy of our field calibration.

RESULTS AND DISCUSSION

Comparison with Experimental Data. The theoretical results are further compared to experiments available in the literature. Obviously, one could not expect to obtain accurate experimental EPR anisotropic parameters from gaseous methyl radicals due to the inevitable effect of the rotational averaging of the anisotropy. That is why the only way of analyzing the theoretical results is to compare to measurements of matrix-isolated methyl radicals. The present qc computations of the **A**- and **g**-tensor components of the methyl radical in vacuum allows, for the first time, elucidating matrix effect on the EPR parameters.

The matrix shifts data listed in Table 8 are calculated based on the results for matrices consisting of linear molecules (Table 5), obtained by Benetis and Dmitriev.[21,24] One could immediately observe almost no matrix effect on the **g**-tensor parallel component which yields a shift 1 order of magnitude below that of the perpendicular component, Table 8. As a result, the parallel **g**-tensor component stays close to the free electron *g*-factor value even for the trapped CH_3 radical. As opposed to $\delta g_{\parallel}$, the perpendicular **g**-tensor component does show appreciable matrix effect whose value, however, is almost identical for all four matrices and is hard to be linked to certain matrix properties.

On the other hand, the **A**-tensor components gradually decrease as the interaction between the CH_3 radical and the matrix molecules grows (Benetis and Dmitriev[21,24]). It is worth noting that the $\delta g_{\perp}$ shift is negative. This effect is expected when the spin−orbit coupling between the unpaired electron and the impurity states of the valence electrons of the matrix molecules is taken into account.

The large **g**-tensor anisotropy of the free methyl radical, $\Delta g^{free} = g_{\parallel} - g_{\perp} = -7.62 \times 10^{-4}$ results in unsplit and largest in amplitude outer $M_F = -3/2$ component, compared to the other hf transitions. For the trapped radical, the decreased $\delta g_{\perp}$ and the unchanged $\delta g_{\parallel}$ bring about a reduced **g**-tensor anisotropy with consequence an unsplit and strongest in amplitude inner $M_F = -1/2$, instead of the $M_F = -3/2$ component. This effect is observed in almost all matrices studied so far, where anisotropy is visible. In Figure 17 is shown a gradual change in the shape of the *A*-line quartet as the matrix shift $-\delta g_{\perp}$ grows in magnitude from 0 to 0.018% which is characteristic of CH_3 in matrices of linear molecules, e.g., N_2, CO, N_2O, and CO_2. The **A**-tensor components and $g_{\parallel}$ are set equal to the values computed for methyl radical in vacuum.

In general Figure 17 testifies a good correlation between the theoretical and experimental results for the EPR lineshape of methyl radical. A similar comparison between the theory and experiment for the EPR of CF_3 radical is not as "comfortable". The fact of the matter is that literature does not provide experimental data with sufficient resolution or signal-to-noise ratio for a reasonable variety of matrices to allow any assumption about the matrix effect on the EPR parameters of the trapped radical. Moreover, available experimental spectra are rather different in several lineshape features, a matter which is clearly seen from comparison of Figures 15 and 18.

In the latter case, Allayarov et al.[29] reported axially symmetric **A**- and **g**-tensors with $A_{\parallel} = 25.15$ mT, $A_{\perp} = 9.1$ mT and $g_{\parallel} = 1.9996$, $g_{\perp} = 2.0056$. The stick diagram in Figure 18 shows only the *A*-symmetry quartet. However, the *E*-symmetry doublet should also contribute to the EPR spectrum of this classical rotor already for much lower temperatures than 77 K; see Rogers and Kispert.[19] While the spectrum symmetry evident from Figure 18 verifies the axial parameters, the simulation should be repeated to take into account a contribution from the second-order doublet.

DOI: 10.1021/acs.jpca.5b05648
J. Phys. Chem. A 2015, 119, 9385−9404

Table 7. *g*-Factors for Several Solid Gas Matrices According to Relevant Literature Data[a,b]

matrix	Ne	Ar	H_2	Kr	CH_4
g-factor	2.002526 (13)[c]	2.002322(56)[c]	2.002516(60)[c]	2.001655(36)[c]	2.00317(≈10)[h]
		2.0022[d]	2.00266(8)[f]	2.001282[g]	2.00242(8)[f]
		2.002110[e]			
		2.00203(8)[f]			
matrix	CO	N_2	N_2O	CO_2	silica gel
g-factor	2.00249 (12)[i]	2.00250(12)[i]	2.00254(12)[i]	2.00248(12)[i]	2.0026(2)[k]
	2.00217(≈10)[j]	2.00217(≈10)[j]		2.00213(≈10)[j]	2.0026(5)[l]
matrix	zeolite	vycor glass	beryl	methane hydrate	liquid methane
g-factor	2.0026[m], 20028[m]	2.0024(1)[p]	2.00254[q]	2.0024(5)[r]	2.00255[s]
	2.00317(≈10)[m]				
	2.0026[n]				
	2.0029[o]				
matrix	Xe	feldspar			
g-factor	2.0020(1)[t]	2.00427(≈10)[u]			
		rhombic **g**-tensor!			

[a]Compare to the computed *g*-factor = 2.002739 for methyl in vacuum in the present work. [b]In case of the axially symmetric **g**-tensor, $g_{iso} = [(2g_\perp + g_\parallel)/3]$. [c]Present study for the sample temperatures, 4.2 K, in Ne, 4.2−26 K, in Ar, 4.2 K, in H_2, 4.2−32 K, in Kr. The magnetic field was well-calibrated using the electron cyclotron resonance line position in magnetic field equal to "*g*" = 1.99987(12). [d]Cirelli, M., et al. *Chem. Phys. Lett.* **1982**, *92*, 223. [e]Popov et al.[37] [f]Jen, C. K. *Phys. Rev.* **1958**, *112*, 1169. [g]Kiljunen, T. *J. Chem. Phys.* **2009**, *130*, 164504. [h]Morehouse, R. *J. Chem. Phys.* **1966**, *45*, 1751. [i]Dmitriev et al.[24] [j]Kiljunen, T., et al. *J. Phys. Chem. A.* **2010**, *114*, 4770. [k]Shiga, T.; Lund, A. *J. Phys. Chem.* **1973**, *77*, 453. [l]Stesmans et al.[27] [m]Danilczuk, M. *Nukleonika* **2005**, *50*, S51. [n]Noble, G. A., et al. *J. Phys. Chem.* **1967**, *71*, 4326. [o]Shiotani, M., et al. *J. Phys. Chem.* **1975**, *79*, 2669 (abnormal radicals). [p]Fuijimoto, M., et al. *Science.* **1966**, *154*, 381. [q]Andersson, L. O. *Phys. Chem. Minerals* **2008**, 10.1007/s00269-008-0245-3. [r]Takeya, K. *Appl. Radiat. Isotopes* **2005**, *62*, 371. [s]Fessenden, R. W.; Schuler, R. H. *J. Chem. Phys.* **1963**, *39*, 2147. [t]Jackel and Gordy.[18] [u]Petrov, I. *J. Am. Mineral.* **1994**, *79*, 221.

Table 8. Relative Matrix Shifts of the EPR Parameters of the CH_3 Trapped in Matrices of Linear Solid Gas Molecules[a]

matrix	$\delta A_\parallel$	$\delta A_\perp$	$\delta g_\parallel$	$\delta g_\perp$
N_2	0.897	1.008	0.0009	−0.0186
CO	0.046	0.707	−0.0015	−0.0181
N_2O	−1.522	−0.003	0.0029	−0.0161
C_2O	−1.567	0.005	−0.0040	−0.0176

[a]The relative shifts are defined as $\delta P_i\% = 100(P_i^M - P_i^{free})/P_i^{free}$ where $P = g, A$; $i = \perp, \parallel$, M = N_2, CO, N_2O, and CO_2.

DISCUSSION

The anisotropy of the α-proton to a π-carbon in Figure 1 of the present work appears to be similar to the figure of the malonic acid π-electron radical showing the principal values and the directions for α-^{1}H dipolar hyperfine coupling tensor in Lund et al.[2] This is very similar to the work by Kubota et al.,[10] a rare report of orthorhombic hfs for CH_3, applying also in our experimentally observed nonrotating satellites[21] and in Kiljunen et al. work; see Table 6. The question is if this effect could be enhanced in $CD_3COONa{\cdot}3D_2O$.

The present comparison of CH_3 with CF_3 EPR simulations is necessary for showing the applicability of the 1Q/2D (one quartet two doublets) method in similar systems. In the article by Benetis and Dmitriev,[6] it was stated that classical behavior of the spin−rotation coupling applies in the CF_3 radical. As explained there, the CH_3 in Ar matrix has very little residual anisotropy due to quantum effects, while those effects might not occur for CF_3 due to the ca. 25-fold greater moment of inertia about its C_3 axis. It is therefore questionable if it is correct to superimpose separate spatial averages of the axially symmetric *A*-quartet and the two *E*-doublets within the C_3 symmetry for the ^{19}F hfs. It seems, however, that the straightforward simulation with applying sequential interaction of nearly axial hfs proton tensors with nonparallel axes agrees quite well with experimental spectra of CF_3 in Kr in Maruani et al.[8,9] However, the simultaneous spatial averaging of the 1Q/2D method within the C_{3v} group is presently closest to the experimental spectrum so far (Figures 15 and 16) but is further studied by appropriate new programming.

We mention here also the Arxiv version of a paper by Shkrob et al.[30] devoted to the radicals in irradiated ionic liquids. Among other radicals, they present EPR spectra of the CF_3 radical in various polycrystalline solids. Figures 4 and 5 of that work are of particular interest. In Figure 4b, one could see the results obtained in radiolysis and photolysis experiments which testify the axial symmetry of the EPR lineshapes. Shkrob et al.[30] stress that their matrices provide rather rigid EPR with a small average. The powder spectrum of trifluoromethyl in the Figure 4S in Shkrob et al.[30] was simulated using the hfcc parameters obtained from DFT calculation, while isotropic **g**-tensors were assumed for all of the radicals. Figure 4S in Shkrob et al.[30] shows in no means a spectrum with axially symmetrical **A**-tensor. However, one wonders if this is a simplification, like the isotropic **g**-tensor or the DFT calculation, suggesting the **A**-tensor axial symmetry. The authors provide, namely, no result of the DFT calculation of the CF_3 radical. These data are announced to be in the appendix of their article, while no appendix could be found. So the reader cannot be sure about whether the axial symmetry of the hf follows exactly from the DFT calculation or this is only simplification.

Finally, we would like to discuss the sample preparation of both the CH_3 vs the CF_3 radicals, related to the above differences in the EPR lineshape of CF_3 reported by different groups. All groups used certain kind of irradiation: X-irradiation of trifluoroacetamide crystal by Kalyanaraman and Kispert;[31] UV-irradiation of CF_3I in rare gases, Maruani et al.;[8] 1-MeV electron bombardment of trifluoroacetamid crystal, Rogers and Kispert;[19] photolysis of $[(CF_3)_2CF]_2$ C_2F_5 radicals in a hexafluoropropylene trimer matrix in Allayarov et al.;[29] photolysis of hexafluoroacetone adsorbed on 13X zeolite in Svejda;[32] and γ-irradiation of CF_4 in solid Xe, Florin et al.[33] In

DOI: 10.1021/acs.jpca.5b05648
J. Phys. Chem. A 2015, 119, 9385−9404

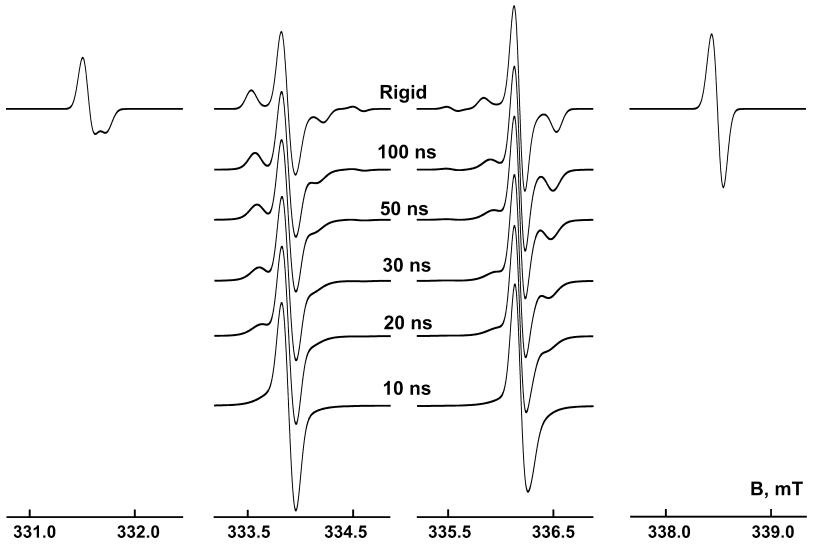

Figure 19. EPR lineshape of the CH_3 radical versus the correlation time of the radical rotation around the 3-fold symmetry axis.[13,36] The microwave resonance frequency was f_{res} = 9391 MHz. The parameters were those used in the previous simulation in Figure 10, left panel. However, the rigid spectrum in this figure is a superposition of the quartet and the doublets with totally equal intensities obtained by double integration.

all experiments, except that by Florin et al., the CF_3 radical is expected to be the one and only dissociation product mobile enough to leave a matrix cage.

However, CF_3 is a rather heavy particle with atomic mass 69 being almost 5 times larger than that of CH_3. One may suggest that it immediately loses its kinetic energy and is trapped nearby the starting point; i.e., the defect site formed after the dissociation. Indeed, Kalyanaraman and Kispert[31] performed computations based on the parent crystal structure and found that CF_3 initially migrates 1.4 Å and then relaxes to near its original molecular position. In that case, the free molecule approximation for CF_3 can be applied depending on how far from its original position the radical is trapped, i.e., on whether the radical surrounding is regular enough. It is well-known that, even for CH_3, different experimental techniques (deposition and irradiation) yield somewhat different results when considering the hindrance of the rotation. This may be the reason for the large anisotropy in Maruani's experiment.[8]

The Effect of Rotation. Since the *EasySpin* "*chili*" function accounting for the molecular rotation did not work properly with the Cartesian 3 × 3 hf tensor format, the CH_3/CF_3 simulations of the rotating molecules were reconsidered using the diagonal elements (eigenvalues) of the **A**- tensors and the corresponding Euler angles in the alternative input format allowed by *EasySpin*. Simulated spectra using these Euler angles were obtained, visualizing how the EPR lineshapes of the "non-rotating-radical" doublets transform into a single *E*-symmetry doublet as the rotation starts and increases in rate.

To our understanding, the opposite temperature behavior of the weak and the strong doublet transitions, as presented in the discussion about Figure 10, gives a hint about the origin of the weak doublet (nonrotating-radical) transitions. The temperature dependence may be explained by one of the following mechanisms, or by their combination.

The rigid spectrum in Figure 19 is a superposition of the quartet and the doublet with equal intensities obtained by double integration. Evidently, the quartet, which is axially symmetric, shows no change in the lineshape by the rotation about the 3-fold axis. For this reason, the two outer lines are not shown in the simulation of the rotating radical. On the one hand, the simulation suggests that, indeed, the intensity of the weak additional resonances decreases, while the two main inner lines increase when the rotation goes faster. On the other hand, the weak resonances, in the simulation, change resonance position in the magnetic field with increasing rotation rate. Notice also some unusual characteristics, such as the asymmetric arrangement about the allowed transitions, and the disappearance of the satellites for higher temperatures, an indication of decreasing influence of quantum effects.[4] This is also observed experimentally for temperatures higher than 10 K in Buscarino et al.,[34] Figure 2, and to 30 K in our Figure 11.

This important difference may suggest that the first mechanism which is based on disregarding rotation and accepting instead that libration do governs the relative intensities of the weak and main inner lines.[35] First at low enough temperatures, the CH_3 radicals perform librations, which after the Knight[5] case of molecular hydrogen positive ions, are suggested to be of *A* and *E*-symmetry, thus giving rise to the simulated spectrum depicted in Figure 10, left panel.

With increasing temperature, a fraction of the radicals start to rotate. The EPR simulation for the CH_3 radical performing fast rotation about the 3-fold axis shows no weak resonances. In particular, as the temperature further increases, the fraction of the rotating radicals increases while the librating radicals' fraction drops. As a consequence, the two main inner lines gradually increase, while the weak resonances disappear.

The temperature-dependent weak transition intensities may be attributed to a gradual change of the rate of the radical rotation around the 3-fold axis. This assumption was verified by simulating the EPR spectra for the axially symmetrical rotation of the CH_3 at different rates; see Figure 19.

A similar response of the radical rotation to the CF_3 spectrum, in particular the correct transformation of the quartet into the mere doublet recorded in the experiment by Maruani et al.,[8] was also obtained preliminarily by the present work.

Comparing CH_3 to CF_3 EPR Simulations. The general *EasySpin* simulation in Figure 16a, where the numerically simulated powder spectrum of the rigid CF_3 was considered taking into account explicitly the separate hf interactions for the

DOI: 10.1021/acs.jpca.5b05648
J. Phys. Chem. A 2015, 119, 9385−9404

three fluorine ^{19}F nuclei, matches rather well the experimental lineshape by Maruani et al.[8] The same standard approach was tested for the CH_3 radical in Figure 20. Comparing this figure

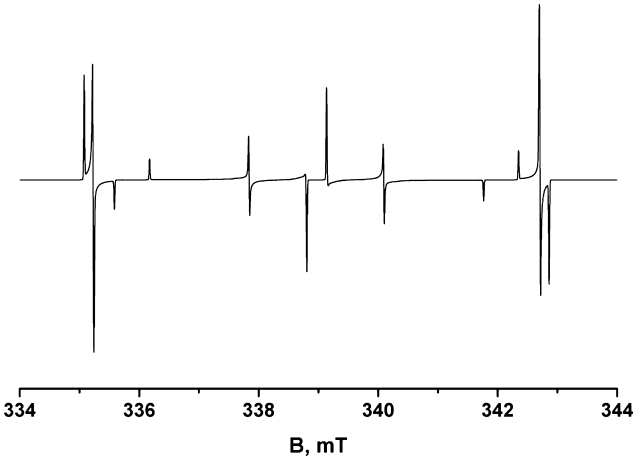

Figure 20. Simulated EPR spectrum of the rigid CH_3 radical obtained by considering three proton ^1H nuclei separately interacting with the unpaired electron. The nuclei have the corresponding symmetry related principal axes for each of them. Each nucleus has hf principal values A_{xx} = −104.4 MHz, A_{yy} = −63.7 MHz, and A_{zz} = −25.96 MHz, with Euler angles $\mathbf{R}_{1R}$ = (90.00, 90.08, −90.00), $\mathbf{R}_2$= (90.00, 89.92, 150), and $\mathbf{R}_3$ = (90.00, 90.00, −150), respectively, in the principal molecular frame (the parallel-direction along the 3-fold symmetry axis) and isotropic *g*-factor = 2.002320. The individual lines were Gaussians of 0.15 G width. The microwave resonance frequency was 9.5 GHz. Second-order perturbation in the computation of the spectrum was applied using the *EasySpin* "*perturb2*" function, because, surprisingly, the "*matrix*" routine of *EasySpin* gave unexpectedly "noisy" spectrum with a great deal of nonaveraged resonances(!).

to both the simulation by superimposed multiplets and the experimental result, Figure 4 and Figure 17, one deduces that the independent nuclei approach is by no means applicable to the CH_3 EPR lineshape simulation.

Such different results for the two trapped radicals, CH_3 and CF_3, deserve special attention. Actually rotation, as studied above, will not be relevant considering the disagreement of the numerical powder simulations of the three separate hf interactions compared to our new 1Q/2D method. More study is necessary in the proposed special powder average computation of CF_3, but it can be left out for the moment. The light CH_3 molecule is a quantum particle, while the heavier CF_3 is a classical particle. The interaction between a guest molecule with the matrix shifts the rotational energy levels of the molecule inversely proportionally to the molecule inertia, to first approximation.

Thus, the shift of the small rotational inertia for a quantum particle is insignificant, and the rotational level sequence is only slightly changed.

On the contrary, for classical molecules with large moment of inertia, the rotational parameters are considerably shifted from the theoretical vacuum values. Furthermore, in the classical case, the moment of inertia becomes less and less relevant for the rotary behavior as the temperature increases. The diffusion constant is instead coming into consideration as the reorientation, so-called tumbling, is ruling the rotational motion. It is in addition known, from previous EPR studies of methyl radical[6,20,37] that the "radical-matrix" interaction of CH_3 in the *E*-symmetry rotational states is significantly larger than for the radical in the *A*-symmetry states.

In case of the trapped CF_3 this effect may lead to considerably different effective inertia I_{eff} for different rotational levels and even to mixing of these levels. One may speculate, in this case, that an EPR spectral analysis should suggest either uncoupled nuclear spin and molecular rotational states or should account for the symmetry of the matrix surroundings when considering symmetry transformations of the molecule. It is worth noting, that the applicability of the new 1Q/2D (one quartet-two doublets) simulation to a given CX_3 for planar molecules in a given matrix would, in addition be a measure of the molecular rotational state "quantumness" vs "guest-host" interaction.

An indirect support for the above suggestion comes from SiH_3 radical. The literature evidence axially symmetrical EPR for this pyramidal (like CF_3) radical with small inertia about the central atom, trapped in various matrices.[38−42]

CONCLUSIONS

Comparing the simulation of the EPR spectra of the trapped CH_3 and CF_3 radicals, it is suggested that, while the matrix effect on the quantum CH_3 rotor is just a perturbation, it may (depending on a matrix used) break the coupling between the CF_3 nuclear spin- and quantum rotational states, thus crucially rearranging the CF_3 EPR lineshape.

The quantum chemistry computation of the EPR parameters of CX_3 (X = H, F) radicals in vacuum undertaken in the present study gives magnetic parameter in satisfactory agreement with the experimental ones in the case of planar CH_3 radical and also in the pyramidal CF_3 radical. The remaining disagreement in the hf interaction parameters is most probably due to the matrix effect on the radical which is beyond the aim of the present study. The simulated lineshape by considering the hf interaction from the point of view of the electron spin is still requiring additional effort in order to reproduce the experimental spectra of the pyramidal CF_3 radical. The analytical derivation reducing the three hf interactions of the proton/fluorine atoms to a quartet and two doublets, 1Q/2D, reveals immediately the main low temperature quantum spectrum but requires a proper superposition for the nonplanar case. However, additional experimental EPR study and simulation of systems such as SiH_3 can adapt the method in order to separate the cases where similar radicals are planar or not. The axial symmetry of the **A**-tensors of the *A*-lines and the **g**-tensors which follow from the present computation were also stressed. The conclusions in an early comprehensive work by Maruani et al.[8] on the trifluoromethyl radical are almost identical with the basic arguments of the present study. In particular they indicate that the above radical at 4.2 K is not rotating, nor inverting as we also indicate. They observe the extreme sidebands that are important for the accurate determination of the hf-parameters as we also do. They also verify partly our conclusions that the tensors are axial, although they state that they did not expected that fact. However, considering the minimal overall $\mathbf{C}_3$ symmetry of the radical, our meaning is that this symmetry should be expected for the hf interaction of the C-13 and for the unpaired electron interaction with the *A*-proton quartet, even if the contributing hf protons interaction do not need to have the same $\mathbf{D}_3/\mathbf{C}_{3v}$ symmetry. However, the hf interactions with the two *E*-symmetry protons in CH_3 and the fluorine doublets in CF_3 are allowed to be nondiagonal. We finish with their citation "...the

DOI: 10.1021/acs.jpca.5b05648
J. Phys. Chem. A 2015, 119, 9385−9404

splitting of the "degenerate" peaks in the experimental spectrum, as well as the nearly axial symmetry of the tensors obtained for the CF_3 radical... are not fully understood".

■ ASSOCIATED CONTENT

Supporting Information

The Supporting Information is available free of charge on the ACS Publications website at DOI: 10.1021/acs.jpca.5b05648.

Construction of the symmetric nuclear spin multiplets of the hf part of the spin Hamiltonian is described in detail in section S1. In section S2, the nature of the least split doublet of the CH_3 EPR spectrum is described (PDF)

■ AUTHOR INFORMATION

Corresponding Author

*E-mail: niben@teiwm.gr. Tel.: +30-24610-68290. Fax: +30-24610-39682. Mob.: +30-693-865 79 69.

Notes

The authors declare no competing financial interest.

■ ACKNOWLEDGMENTS

Y. D. acknowledges partial support by the Russian Foundation for Basic Research (RFBR), research project no. 13-02-00373a. We would like to thank Professor Anders Lund for his invaluable help and encouragement during this study.

■ REFERENCES

(1) McConnell, H. M.; Strathdee, J. Theory of Anisotropic Hyperfine Interactions in p-electron Radicals. *Mol. Phys.* **1959**, *2*, 129−38.

(2) Lund, A.; Shiotani, M.; Shimada, S. *Principles and Applications of ESR Spectroscopy*; Springer: New York, 2011; Section 2.2.2.1, The measurement of ^1H hyperfine coupling (hfc) tensors.

(3) Carrington, A.; MacLauchlan, A. D. *Introduction to Magnetic Resonance. With applications to Chemistry and Chemical Physics*; Harper and Row: New York, 1967.

(4) Yamada, T.; Komaguchi, K.; Shiotani, M.; Benetis, N. P. Sørnes High Resolution EPR and Quantum Effects on CH_3, CH_2D, CHD_2 and CD_3 Radicals under Argon-matrix Isolation Conditions. *J. Phys. Chem. A* **1999**, *103*, 4823−4829.

(5) Correnti, M. D.; Dickert, K. P.; Pittman, M. A.; Felmly, J. W.; Banisaukas, J. J., III; Knight, Jr.; Lon, B. Electron Spin Resonance Investigation of H_2^+, HD^+, and D_2^+ Isolated in Neon Matrices at 2 K. *J. Chem. Phys.* **2012**, *137*, 204308.

(6) Benetis, N. P.; Dmitriev, Y. Inertial Rotation and Matrix Interaction Effects on the EPR Spectra of Methyl Radicals Isolated in 'Inert' Cryogenic Matrices. *J. Phys.: Condens. Matter* **2009**, *21*, 103201−22.

(7) Freed, J. H. Quantum Effects of Methyl-Group Rotations in Magnetic Resonance: ESR Splitting and Linewidths. *J. Chem. Phys.* **1965**, *43*, 1710.

(8) Maruani, J.; McDowell, C. A.; Nakajima, H.; Raghunathan, P. The Electron Spin Resonance Spectra of Randomly Oriented Trifluoromethyl Radicals in Rare-Gas Matrices at Low Temperatures. *Mol. Phys.* **1968**, *14*, 349−366.

(9) Maruani, J.; Coope, J. A. R.; McDowell, C. A. Detailed Analysis of the Singularities and Origin of the Extra Lines in the E.S.R. Spectrum of the $^{\bullet}CF_3$ Radical in a Polycrystalline Matrix. *Mol. Phys.* **1970**, *18*, 165−176.

(10) Kubota, S.; Iwaizumi, M.; Ikegami, Y.; Shimokoshi, K. Anisotropic Hyperfine Interaction in the Electron Spin Resonance Spectrum of the Methyl Radical Trapped in $CH_3COONa \cdot 3D_2O$ Crystal at Low Temperatures. *J. Chem. Phys.* **1979**, *71*, 4771−4776.

(11) Lee, J. Y.; Rogers, M. T. Tunneling Rotation of the Methyl Radical in Solids. *J. Chem. Phys.* **1976**, *65*, 580−581.

(12) Barbon, A.; Brustolon, M.; Maniero, A. L.; Romanelli, M.; Brunel, L.-C. Dynamics and Spin Relaxation of Tempone in a Host Crystal. An ENDOR, High Field EPR and Electron Spin Echo Study. *Phys. Chem. Chem. Phys.* **1999**, *1*, 4015−23.

(13) EASYSPIN, free Matlab software written by Stoll S.: http://www.easyspin.org/. Two of the usual software were available, the *WinEPR* and the *EasySpin*. The latter is applicable when one deals with the effect of radical rotation on the EPR spectrum and/or exact diagonalization. On the contrary, in this case of lacking motional dynamics, it is much easier to perform EPR spectral simulations using the WINEPR software, according to the second-order perturbation approach.

(14) *Gaussian 09*, Revision A.02; Frisch, M. J.; Trucks, G. W.; Schlegel, H. B.; Scuseria, G. E.; Robb, M. A.; Cheeseman, J. R.; Scalmani, G.; Barone, V.; Mennucci, B.; Petersson, G. A., et al., Gaussian, Inc.: Wallingford, CT, 2009.

(15) Schreckenbach, G.; Ziegler, T. Calculation of the G-Tensor of Electron Paramagnetic Resonance Spectroscopy Using Gauge-Including Atomic Orbitals and Density Functional Theory. *J. Phys. Chem. A* **1997**, *101*, 3388−3399.

(16) Vahtras, O.; Engström, M.; Schimmelpfennig, B. Electronic g-Tensors Obtained with the Mean-Field Spin−Orbit Hamiltonian. *Chem. Phys. Lett.* **2002**, *351*, 424−430.

(17) Helgaker, T.; Jaszuński, M.; Ruud, K. Ab Initio Methods for the Calculation of NMR Shielding and Indirect Spin-Spin Coupling Constants. *Chem. Rev.* **1999**, *99*, 293−352.

(18) Jackel, G. S.; Gordy, W. Electron Spin Resonance of Free Radicals Formed from Group-IV and Group-V Hydrides in Inert Matrices at Low Temperature. *Phys. Rev.* **1968**, *176*, 443.

(19) Rogers, M. T.; Kispert, L. D. Trifluoromethyl, and Other Radicals, in Irradiated Single Crystal of Trifluoroacetamide. *J. Chem. Phys.* **1967**, *46*, 3193−3199.

(20) Dmitriev, Y. A.; Benetis, N. P. EPR Line-Shape Anisotropy and Hyperfine Shift of Methyl Radicals in Solid Ne, Ar, Kr, and p-H_2 Gas Matrices. *J. Phys. Chem. A* **2010**, *114*, 10732−10741.

(21) Benetis, N. P.; Dmitriev, Yu Anomalous EPR Intensity Distribution of the Methyl Radical Quartet Adsorbed on the Surface of Porous Materials. Comparison with Solid Gas Matrix Isolation. *J. Phys. Chem. A* **2013**, *117*, 4233−4250.

(22) Following Prof. Anders Lund, private communications and Erickson, R.; Lund, A. *Applications of EPR and ENDOR Spectrum Simulations in Radiation Research*; Ch. 19 in Applications of EPR in Radiation Research; Springer: New York, 2014; pp 703−749.

(23) Davis, S.; Anderson, D. T.; Duxbury, G.; Nesbitt, D. J. Jet-Cooled Molecular Radicals in Slit Supersonic Discharges: Sub-Doppler Infrared Studies of Methyl Radical. *J. Chem. Phys.* **1997**, *107*, 5661.

(24) Dmitriev, Yu.A.; Melnikov, V. D.; Styrov, K. G.; Tumanova, M. A. EPR Study of Methyl Radical in Van-der-Waals Solids. *Phys. B* **2014**, *440*, 104−112.

(25) Dmitriev, Yu.A. High-Resolution EPR and the Origin of the Spectrum Anisotropy of CH_3 Radicals in Ar, Kr, and CO Matrices at Liquid Helium Temperatures. *Phys. B* **2004**, *352*, 383−389.

(26) Edlund, O.; Lund, A.; Shiotani, M.; Sohma, J.; Thuomas, K.-Å. Theory for the Anisotropic Hyperfine Coupling with Fluorine: the $\cdot CF_3$ Radical. *Mol. Phys.* **1976**, *32*, 49−69.

(27) Stesmans, A.; Clémer, K.; Afanas'ev, V. V. Electron Spin Resonance Probing of Fundamental Point Defects in Nanometer-Sized Silica Particles. *Phys. Rev. B: Condens. Matter Mater. Phys.* **2005**, *72*, 155335.

(28) Dmitriev, Yu.A.; Zhitnikov, R. A. EPR Study of Methyl Radicals. Anisotropy and Tumbling Motion in Low Temperature Matrices. *J. Low Temp. Phys.* **2001**, *122*, 163−170.

(29) Allayarov, S. R.; Chernysheva, T. E.; Mikhailov, A. I. ESR Spectra of Trifluoromethyl Radical Obtained by Radiolysis and Photolysis in Solid Matrices. *High Energy Chem.* **2002**, *36*, 152−156.

(30) Shkrob, I. A.; Chemerisov, S. D.; Wishart J. F. *EPR Study of Radicals in Irradiated Ionic Liquids and Implications for the Radiation Stability of Ionic Liquid-Based Extraction Systems*, version 3; Office of

DOI: 10.1021/acs.jpca.5b05648
J. Phys. Chem. A 2015, 119, 9385−9404

Science, Division of Chemical Science, US-DOE: Washington, DC, 2007.
(31) Kalyanaraman, B.; Kispert, L. D. The ESR Study of the CF_3 F Radical in Irradiated Trifluoroacetamide Single Crystals. *J. Chem. Phys.* **1978**, *68*, 5219−5224.
(32) Svejda, P. Electron Spin resonance Study of Adsorption Stabilization of Photolytic Trifluoromethyl Radicals on Zeolite. *J. Phys. Chem.* **1972**, *76*, 2690−2693.
(33) Florin, R. E.; Brown, L. A. Wall γ- Irradiation of Small Molecules at 4 and 77 K. *J. Phys. Chem.* **1962**, *66*, 2672−2676.
(34) Buscarino, G.; Alessi, A.; Agnello, S.; Boizot, B.; Gelardia, F. M.; Boscaino, R. Isolation of the CH_3 Rotor in a Thermally Stable Inert Matrix: First Characterization of the Gradual Transition from Classical to Quantum Behavior at Low Temperatures. *Phys. Chem. Chem. Phys.* **2014**, *16*, 13360.
(35) Vorobiev, A. Kh.; Chumakova, N. A. *Simulation of Rigid-Limit and Slow-Motion EPR Spectra for Extraction of Quantitative Dynamic and Orientational Information*, Chap. 3. Nitroxides - Theory, Experiment and Applications;Kokorin, A. I., Ed.; Intech, 2012; 10.5772/74052
(36) We note that simulations of the CH_3 and CF_3 lineshapes that follow best the lineshape transformation by rotation of the radicals are obtained using the *EasySpin* software than WINEPR.
(37) Popov, E.; Kiljunen, T.; Kunttu, H.; Eloranta, J. Rotation of Methyl Radicals in a Solid Argon Matrix. *J. Chem. Phys.* **2007**, *126*, 134504.
(38) Adrian, F. J.; Cochran, E. L.; Bowers, V. A. ESR Studies of Inorganic Free Radicals in Photolytic Systems. In *Advances in Chemistry Series*; Gould, R. F., Ed.; American Chemical Society: Washington, DC, 1962.
(39) Nakamura, K.; Masaki, N.; Sato, S.; Shimokoshi, K. Free Radicals Formed by Reaction of Silane with Hydrogen Atoms in Rare Gas Matrices at Very Low Temperatures. *J. Chem. Phys.* **1985**, *83*, 4504−4510.
(40) Nakamura, K.; Okamoto, M.; Takayanagi, T.; Kawachi, T.; Shimokoshi, K.; Sato, S. Electronic Spin Resonance Spectra of SiH_3 Radicals Trapped in the Low Temperature Matrix of Nonmagnetic Isotopes of Xenon. *J. Chem. Phys.* **1989**, *90*, 2992−2994.
(41) Raghunathan, P.; Shimokoshi, K. On the Anisotropic Electron Spin Resonance Spectroscopic Parameters and Motional States of Matrix-Isolated Silyl (SiH_3) Radical at Low Temperatures. *Spectrochim. Acta* **1980**, *36*, 285−290.
(42) Van Zee, R. J.; Ferrante, R. F.; Weltner, W., Jr. Si_2, SiH_3, and HSiO Molecules: ESR at 4 K. *J. Chem. Phys.* **1985**, *83*, 6181−6187.

DOI: 10.1021/acs.jpca.5b05648
J. Phys. Chem. A 2015, 119, 9385−9404